Journal of South American Earth Sciences 66 (2016) 232–247

Contents lists available at ScienceDirect

Journal of South American Earth Sciences

journal homepage: www.elsevier.com/locate/jsames

New records of late Holocene tephras from Lake Futalaufquen (42.8°S), northern Patagonia

Romina Daga [a, b, *], Sergio Ribeiro Guevara [a], María Arribére [a, c]

[a] Laboratorio de Análisis por Activación Neutrónica, Centro Atómico Bariloche, CNEA, Av. Bustillo km 9.5, 8400 Bariloche, Argentina
[b] Consejo Nacional de Investigaciones Científicas y Técnicas (CONICET), Argentina
[c] Instituto Balseiro, UNCu, Av. Bustillo km 9.5, 8400 Bariloche, Argentina

A R T I C L E I N F O

Article history:
Received 17 August 2015
Received in revised form
30 November 2015
Accepted 17 December 2015
Available online 20 December 2015

Keywords:
Tephra
Lake sediments
Southern Volcanic Zone
Patagonia
Argentina

A B S T R A C T

In regions with limited knowledge of the historical volcanic record, like remote areas in the Andean Southern Volcanic Zone, the definition of reliable age-depth models for lake sequences represents a valuable tool for tephra layers dating. In Lake Futalaufquen (42.8°S), Northern Patagonia, a short sedimentary sequence was extracted after the AD 2008 Chaitén eruption with the purpose to analyze the records of volcanic eruptions at these poorly studied latitudes. The sequence was dated by ^{210}Pb, ^{137}Cs, and ^{14}C techniques. Five tephras were identified for the last 1600 years, restricted to the last 5 centuries. Sedimentology, morphology, and geochemical properties allowed the characterization of the tephras and their correlation with tephras recently identified proximal to the sources, mainly from Chaitén and Huequi volcanoes, and Michinmahuida accessory cones, representing the first distal records reported of these tephras. Furthermore, tephras modeled ages obtained by the sequence age-depth model shrink the ages for the volcanic events, like a potential cycle of activity from Michinmauida accessory cones during AD 1530 ± 55, one eruption from Huequi volcano at AD 1695 ± 50, and a possible recent eruption from Chaitén at AD 1775 ± 40. Additionally, the work contributes to improve the regional volcanic records knowledge, basic for volcanic hazard assessment.

1. Introduction

Tephra layers are widely used as time-synchronous horizons, linking and dating different geological, palaeoclimatic, or archaeological archives. This requires detailed tephra characterization of either physical properties evident in the field or morphological, mineralogical, and geochemical analyses performed in the laboratory, obtaining a 'fingerprint' for each tephra layer (Lowe, 2011). The complete characterization is particularly useful when proximal, medial, or distal tephra-fall deposits need to be correlated, usually allowing their association with dated events or with other characterized tephras. This technique is commonly used in active volcanic regions where the high eruptive frequency makes that volcanic deposits become a common component in sedimentary sequences (Steinhauser et al., 2007; Lowe, 2011; Bertrand et al., 2014; Daga et al., 2014). Sometimes, proximal deposits are obliterated by following eruptions, and medial to distal records would help to improve the volcanic record if they are well preserved (Fontaine et al., 2007).

In this way, lakes become the appropriate systems for tephra preservation due to its nearly continuous sediment accumulation, avoiding strong superficial processes, and providing consequently useful records of the lake depositional history, offering exceptional stratigraphical and chronological control (Wulf et al., 2004; Fey et al., 2009; Fontijn et al., 2014). Tephrochronology has proved to be a valuable tool to develop consistent chronological frameworks in sedimentary sequences, being a basic issue for palaeoenvironmental (Shane, 2000; Chambers et al., 2004; Wastegard, 2005) and, mainly in this region, for paleoseismological studies (Moernaut et al., 2014; Van Daele et al., 2015). This technique is particularly useful in Patagonia to date short sedimentary sequences, due to low ^{210}Pb fluxes limiting ^{210}Pb dating method (Ribeiro Guevara et al., 2003; Arnaud et al., 2006). However, in regions frequently affected by volcanic eruptions but poorly studied, where there is an incomplete knowledge of the historical eruptions and its deposits, this kind of correlations between tephras and the volcanic source could be a difficult task. The combined application of dating techniques, as isotope and

* Corresponding author. Av. Bustillo km 9.5, 8400 Bariloche, Argentina.
E-mail address: romina@cab.cnea.gov.ar (R. Daga).

http://dx.doi.org/10.1016/j.jsames.2015.12.003
0895-9811/

radiocarbon methods, could provide high temporal resolution records throughout the Holocene. Such chronological frameworks determined for lake sequences represent a valuable tool in the establishment of tephra layers age due to the application of modern methods as Bayesian analysis (Okuno and Nakamura, 2003; Lowe, 2011; Watt et al., 2011a). These contribute to improve the regional volcanic record knowledge, considered the basis for volcanic hazard assessment.

The Northern Patagonia Andean Range is situated in the Southern Volcanic Zone (SVZ) of the Andes, a region with several active volcanic systems during historical times. Although diverse research works have been carried out, the data available is scarce in many regions of the SVZ regarding the identification and characterization of volcanic events and pyroclastic distribution patterns, not allowing to building a consistent tephrochronological framework in these regions. This is the case of Los Alerces National Park (LANP) and nearby region (Fig. 1). Different studies were prompted at these latitudes mainly after the volcano Chaitén eruption in 2008, improving the knowledge of volcanic events from a considered almost inactive volcano. These recent works recognize pyroclastic deposits from until now unknown eruptions for the last centuries from Yate, Huequi, Chaitén, and Michinmahuida volcanoes (Fig. 1) (Watt et al., 2011a, 2011b, 2013; Amigo et al., 2013; Lara et al., 2013; Moreno et al., 2014). Even though, the geochemical characterization of these recently identified tephras is scarce, and ages are imprecise.

Present research investigates new tephra records in a lacustrine sedimentary sequence extracted from Lake Futalaufquen, in LANP, covering last 1600 years. The sequence was dated with ^{210}Pb, ^{137}Cs and ^{14}C techniques, allowing the chronological framework for a reliable dating of the tephras identified. The sedimentology, mineralogy, morphology, and geochemistry of the primary products isolated from these tephras were analyzed by visual inspection of the sequence, X–ray diffraction, Scanning Electron Microscopy (SEM), and Instrumental Neutron Activation Analysis (INAA), aiming to provide a full characterization to support correlation with volcanic sources.

2. Study site

Lake Futalaufquen (42°49′S, 71°43′W) is an oligotrophic lake located in LANP in the Andean Range, northern Patagonia, at 518 m

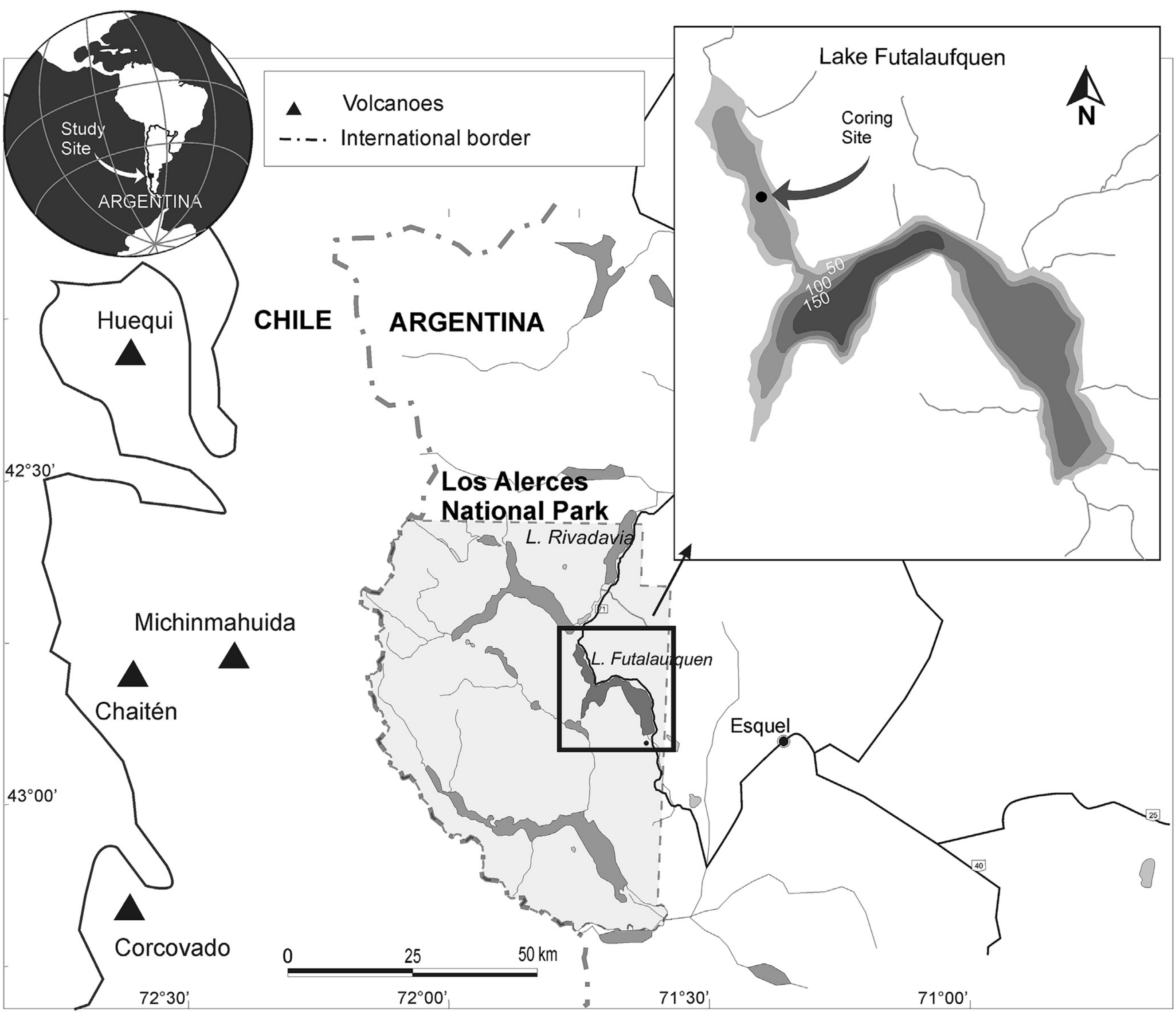

Fig. 1. Location of Lake Futalaufquen in Los Alerces National Park (LANP), Argentina, and its potential volcanic ash sources.

a.s.l. (Fig. 1). It is a water body with several branching arms occupying 44.6 km^2 of old fluvial valleys overdeepened by glacial erosion, in an intermediate position of the Futaleufú basin, reaching a maximum depth of 168 m (Pizzolón, 1995). The lake collects waters from 2920 km^2 of catchment, being the main tributary the Arrayanes river, draining lakes Rivadavia and Menéndez waters, and flowing into the small Lake Kruger. LANP, with approximately 2600 km^2, is a protected area where the anthropogenic activity and the pressure on the system are restricted to the low density population and seasonal tourism, making possible the preservation of the records of regional and/or global impacts on the lacustrine sedimentary sequences. The catchment is characterized by high mountains and the lithology is composed of Jurassic volcaniclastic rocks on the western margin of Lake Futalaufquen, intruded by Cretaceous Andean granitoids identified mainly on the central part of the catchment, and Paleogene vulcanites with associated sedimentites to the easternmost sector (Lizuain, 1999). Valleys are composed of Pleistocene undifferentiated agradational deposits and recent alluvial and colluvial material. The soils of the region are represented by andisols developed in volcanic and/or volcaniclastic material and ustolls from unconsolidated Quaternary materials on gentle to moderate slopes (Del Valle, 1998). Vegetation is dominated by pure or mixed stands of conifer, evergreen, and deciduous species, with shrublands dominating between 1000 and 1200 m a.s.l. High Andean, above the tree-line, is dominated by uncovered rocks with islands of grasses, shrubs, and forbs of limited cover (Vila and Borrelli, 2011).

The Andean Range, in northern Patagonia (around 41–43°S), located in the Southern Volcanic Zone of the Andes (Stern, 2004), results from the subduction of the Nazca Plate under the South American Plate. The current active volcanic arc extends from 33° S to 46° S and includes several active volcanoes from the Miocene to the present. Volcanoes close to the study zone are Huequi, Chaitén, Michinmahuida, and Corcovado (Fig. 1), with few available compilations about the historical volcanic activity (González Ferrán, 1995; Petit-Breuilh Sepulveda, 2004), and limited scientific studies about them. As was observed during the last explosive rhyolitic eruption from Chaitén volcano in 2008, volcanic events occurred in the nearby SVZ have frequently affected the Patagonian territory and the study site in particular.

Climate in this region is defined as cool-temperate humid, with austral fall-winter precipitations. The mean annual temperature is about 8 °C. In Patagonia, climate is dominated by the combination of global circulation patterns, seasonal movements of air masses coming from de Pacific Ocean, and the topographic barrier represented by the Andes parallel to the Pacific coast (Paruelo et al., 1998). While the first ones result in dominant strong and constant west winds across the region, the Andes position generate a strong west-east gradient of precipitations across the region, with more than 2000 mm/yr at the eastern base of the Andes decreasing exponentially to under 200 mm/yr on the steppe (Paruelo et al., 1998; Roig and Villalba, 2008). Consequently, volcanoes belonging to SVZ constitute potential sources of volcanic ashes to the lakes in the study site.

3. Material and methods

3.1. Coring and sampling

A short sediment core of 79 cm length was extracted in 2009 austral summer from Lake Futalaufquen (Fig. 1) with a messenger-activated gravity type corer. The sampling site (42°49′S, 71°43′W) was selected in a flat area of the lake bottom, determined after echo sounder survey. The sediment core was cut longitudinally and subsampled in 1 cm slices (except for tephra layers, in which natural boundaries were kept) after visual inspection. Each subsampled sediment layer was freeze-dried until constant weight was achieved. Physical properties of sediment as water percentage (WP) and dry density (DD) were calculated by weighting wet and freeze-dried subsamples. Determination of loss on ignition (LOI_{550}) was carried out along the sedimentary sequence, in approximately 0.5 g of sample, at 550 °C for 4 h after Heiri et al. (2001), as organic matter indicator (Smol, 2008). Finally, five tephra layers were identified visually by differences in color and grain size, pointed out by anomalies in core physical properties and organic matter (Fig. 2), and confirmed after binocular magnifying glass examination. Tephra layers were labeled by lake code adding the basal depth (cm) in the sequence.

3.2. Chronology

The age-depth model was carried out by ^{210}Pb and ^{137}Cs techniques in upper layers (Joshi and Shukla, 1991; Robbins and Herche, 1993; Ribeiro Guevara and Arribére, 2002; Ribeiro Guevara et al., 2003), and with AMS radiocarbon dates for older layers. ^{210}Pb, ^{226}Ra, and ^{137}Cs specific activity profiles were measured by high-resolution gamma-ray spectrometry (Ribeiro Guevara and Arribére, 2002; Ribeiro Guevara et al., 2003) using a well-type HPGe detector, with self-shielding corrections according to Furci et al. (2013). Given that no macrofossils were available, bulk sediments from two deep layers were selected for AMS radiocarbon dating at University of Georgia (USA). The calibration and integration of the information in the age-depth model was carried out by OxCal 4.2 (available at https://c14.arch.ox.ac.uk/oxcal/OxCal.html), using the Southern Hemisphere radiocarbon calibration data SHCal13 (Hogg et al., 2013) (Table 1). The OxCal 4.2 Bayesian model (Bronk Ramsey, 2009) combines as input parameters the prior information about the sequence (boundaries represented by core bottom and top, order of deposition, and depths) and measurements on the sequence (uncalibrated ^{14}C ages with the respective uncertainty and the calibrated ^{137}Cs point) providing a model that uses such information to constrain the chronology and to provide interpolation between dated levels in any sequence (Bronk Ramsey, 2008). The *P_Sequence* model (which assimilates sedimentation as a random process following a Poisson law; Bronk Ramsey, 2008) was applied with *k* parameter (regularity of the sedimentation) set equal to 2 cm^{-1}, considering that in cores with few changes in sedimentation rate the k value can be increased in order to decrease the uncertainty between the dated depths reducing the 'bowing' effect (Parnell et al., 2011) (model code in Supplementary Information). For the model, core depth was corrected by subtracting tephra layers >1 cm thick, which are assumed instantaneously deposited. Only the most recent tephra identified in the core was included in the model due to the certain correspondence with the 2008 Chaitén eruption. Ages are given as calibrated calendar years AD at the 95.4% (2σ) confidence level (Table 1).

3.3. Morphological and mineralogical characterization

Tephra layers were first described under binocular magnifying glass to identify macroscopic characteristics and to classify the different components in each layer. Afterwards, tephras were sieved (>500 μm, 500–250 μm, 250–125 μm, 125–63 μm, <63 μm fractions). Juvenile volcanic components named white pumice, scoria fragments and glass shards were identified and morphologically characterized under binocular magnifying glass. For a detailed characterization, samples were also mounted on a holder and coated with Au for observations with a Philips 515 SEM at an acceleration voltage of 20 kV.

The qualitative mineralogy of powdered bulk samples was

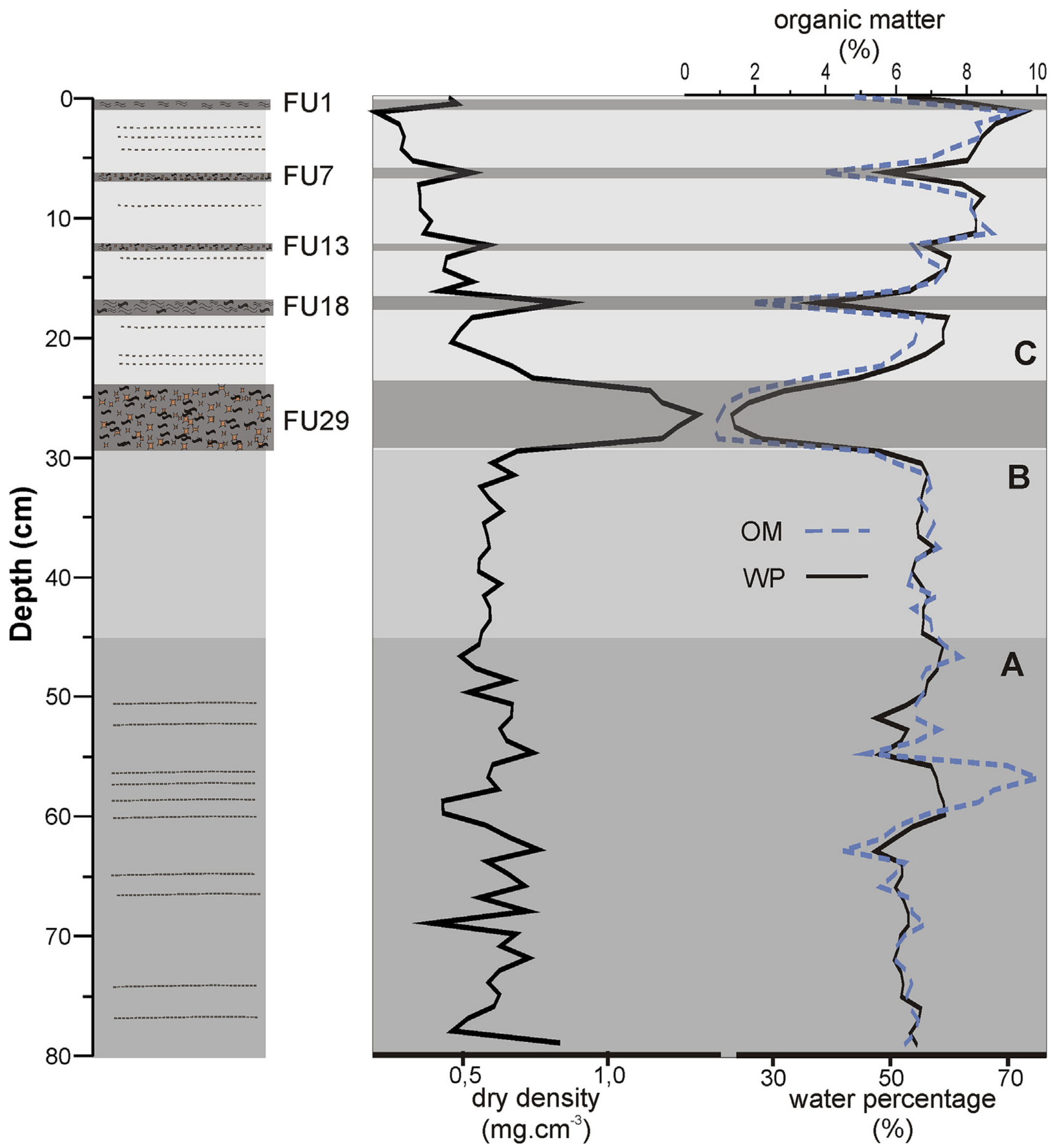

Fig. 2. Synthetic lithological profile with identified Units A, B, and C, and tephra layers from Lake Futalauquen core at left; dry density (DD), water percentage (WP), and organic matter (OM) profiles at right.

Table 1
Calibrated radiocarbon dates from Lake Futalaufquen from age-depth model using OxCal 4.2 (Bronk Ramsey, 2009), and the Southern Hemisphere radiocarbon calibration data SHCal13 (Hogg et al., 2013). Adjusted depth corresponds to depth discarding tephra layers. $\delta^{13}C$ reported by ^{14}C laboratory.

Depth (cm)	Adjusted depth (cm)	Material	Laboratory code	^{14}C age ± 1σ (years BP)	$\delta^{13}C$, ‰	Median probability (cal AD)	Cal age with 2σ range (cal AD)
54	48.5	sediment	UGAMS 8488	1160 ± 25	−27.4	950	890–990
76	70.5	sediment	UGAMS 8489	1620 ± 25	−27.2	485	415–570

analyzed by X–ray diffraction (XRD), using a PANalytical X–ray diffractometer, operating with 40 kV accelerating voltage and 45 mA current, and collecting data between 3 and 60 2θ, by the Grupo de Caracterización de Materiales (Centro Atómico Bariloche).

3.4. Geochemistry

Elemental concentrations were determined on tephra samples for a geochemical characterization allowing the correlation with volcanic sources. The juvenile volcanic components from different grain size fractions (>500 μm, 500–250 μm, 250–125 μm) were identified and isolated under binocular magnifying glass for elemental determinations. The methodology is described in Daga et al. (2006). Elemental concentrations were determined by Instrumental Neutron Activation Analysis (INAA), obtaining the major elements Al, Ca, Fe, Mg, Mn, Na, K, and Ti, rare earth La, Ce, Dy, Nd, Sm, Eu, Tb, Yb, Lu, and other trace elements as Sb, As, Ba, Br, Cs, Zn, Co, Cr, Hf, Sc, Sr, Rb, Ta, Th, U, V, and Zr. Bulk data from different kind of particles (white pumice, scoria, glass shards) on different grain size fractions were obtained. Major elements were converted to oxides and SiO_2 contents were estimated by mass difference. Analytical errors differ for each element and sample analyzed, since they depend on the nuclear parameters of each element, on the irradiation conditions, and on the composition of the sample, varying in most elements from 4 to 12% and increasing for Sr, Br, Cr, and Zr up to around 20%. Certified Reference Materials NIST Buffalo River Sediment and IAEA SL1 Lake Sediment were analyzed together with the samples for analytical quality control.

4. Results

4.1. Chronology construction

Lake Futalaufquen sequence dating was carried out by ^{210}Pb, ^{137}Cs, and ^{14}C techniques. ^{210}Pb and ^{137}Cs dating was performed by evaluation of the specific activity in the upper layers, up to 4.8 g cm^{-2} depth (11–12 cm layer), identifying a tephra layer immediately below that (FU13). At this point, unsupported ^{210}Pb specific activity decreased to negligible values. The uppermost layer is a tephra corresponding to Chaiten 2008 eruption (FU1); another coarse tephra was visually identified at 6–7 cm (FU7), with limited incidence in 5–6 and 7–8 cm. The ^{210}Pb specific activity does not exhibit the exponential profile not allowing the sequence dating (Fig. 3). Therefore, ^{210}Pb dating is not reliable, and it is not consider for the analysis.

^{137}Cs specific activity was below detection limits in layers deeper than 6–7 cm depth. In upper layers, the ^{137}Cs profile shows a clear peak, with a sharp decrease (Fig. 3), allowing the estimation of the sedimentation rate in this section of the sedimentary sequence. The steep decrease could be ascribed to the starting of the relevant ^{137}Cs fallout, assuming the lower point (5–6 cm layer) as mobilization after deposition or minor inputs in previous periods. Accordingly, the uncertainty of the sedimentation rate is estimated by the average of half of the layers 4–5 and 5–6 cm. The relevant ^{137}Cs fallout starting year, associated with the base of the 4–5 cm layer, is 1962. The uppermost layer (0–0.5 cm) is mostly a tephra (from Chaiten 2008 eruption). The sedimentation subsequent to the eruption is less than one year, which could be

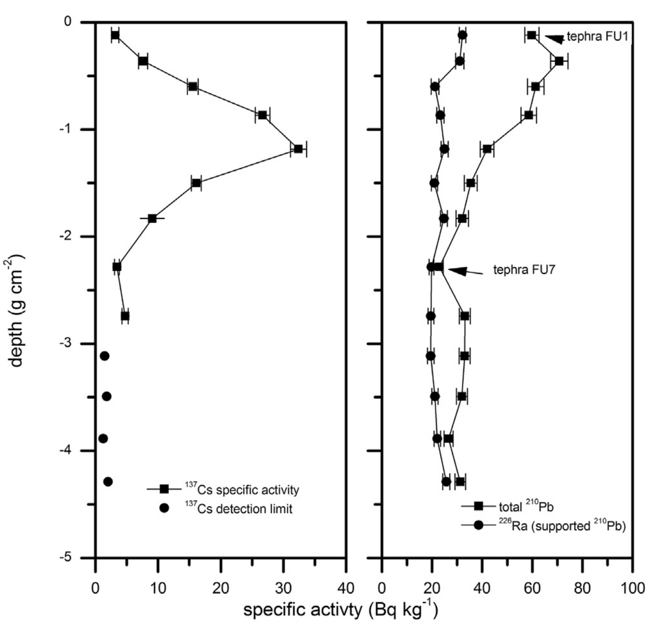

Fig. 3. Specific activity profiles of ^{137}Cs, ^{210}Pb, and ^{226}Ra (in secular equilibrium with supported ^{210}Pb).

estimated as 10% of the layer. On the other hand, there were pyroclastic products identified in the second layer (0.5–1 cm), probably due to mixing during sub-sampling. Corrections due to both considerations were included. Therefore, the estimation of the average sedimentation rate corresponds to a cumulative mass of 30.2 ± 3.5 mg cm^{-2} y^{-1} for the 1962–2009 period.

The two deep layers selected for AMS ^{14}C analysis (Table 1) and ^{137}Cs dates were integrated using OxCal 4.2 (Bronk Ramsey, 2009; ShCal13, Hogg et al., 2013). This allowed to calculate the age of the tephra layers with 68.2% and 95.4% age probability ranges (1σ and 2σ), and also extrapolate the dating to the bottom of the sequence obtaining the time spanned by the core (Fig. 4). Fig. 4 represents the adjusted core depth excluding volcanic layers >1 cm; further analysis considers the real depth of the sequence.

The resultant age-depth model obtained suggests a relatively constant sedimentation rate since AD ~400 (Fig. 4). Accordingly, the AMS ^{14}C dating in deep layer assigned an AD 890–990 date to the 53–54 cm layer, and an AD 415–570 date to the 75–76 cm layer, leading a sedimentation rate in this sequence section of 30.8 ± 4.2 mg cm^{-2} y^{-1}, in very good agreement with ^{137}Cs sedimentation rate in upper layers (30.2 ± 3.5 mg cm^{-2} y^{-1}).

4.2. Core lithology

Sediment sequence lithology is composed mostly of homogeneous to laminated siliciclastic sediment, and low variable organic matter through the profile (LOI_{550} contents less than 10%). Macroscopic features allow the identification of three units (Fig. 2). From bottom to top: Unit A (79-45 cm; AD ~400–1200) is composed of silty-clayed sediment with regular green and black millimetric to centimetric lamination intercalated in the grayish-brown background material, with variable DD; Unit B (45-30 cm; AD ~1200–1500) corresponds to massive, brownish, silty-clayed sediment, with less variable DD and WP; and Unit C (30-0 cm; AD ~1500–2009) consists of laminated silty-clayed to sandy sediment, varying from grayish, brownish, to black color. DD shows a clear decreasing up-core tendency in the background levels of Unit C, followed by the opposite behavior of WP. Strong peaks of DD and WP correspond to the coarser grain-sized layers representing inputs of allochthonous material, i.e. the tephra deposits (Fig. 2), which were only identified in this Unit.

4.3. Tephra deposits

The five tephra layers identified in the sequence are part of Unit C (Fig. 4), and main physical and morphological features are shown in Table 2 and Fig. 5, respectively. These tephras were identified as FU1, a thin coarse grain-sized white pumiceous tephra dispersed at 0–1 cm depth, corresponding to the well known 2008 Chaitén eruption (located <80 km directly to the west of Lake Futalaufquen; Fig. 1); FU7, a mixed layer at 6.5–7 cm depth consisting of white pumice, glass, and scoria fragments; FU13, also a mixed thin layer composed of white pumice, glass, and scoria fragments at 12.7–13 cm; FU18, a coarse grayish-white pumiceous tephra at 16.5–18 cm depth; and FU29, a composite dark layered scoria-glassy tephra at 24–29 cm depth.

4.3.1. Tephra FU1

This deposit corresponds to a scattered tephra at 0–1 cm depth, composed of fine ash with coarser highly vesicular white pumices reaching 500 μm (Fig. 5a), immersed in the oxidized upper centimeters of the core.

4.3.2. Tephra FU7

This fine ash layer (6.5–7 cm depth) was clearly identified due to

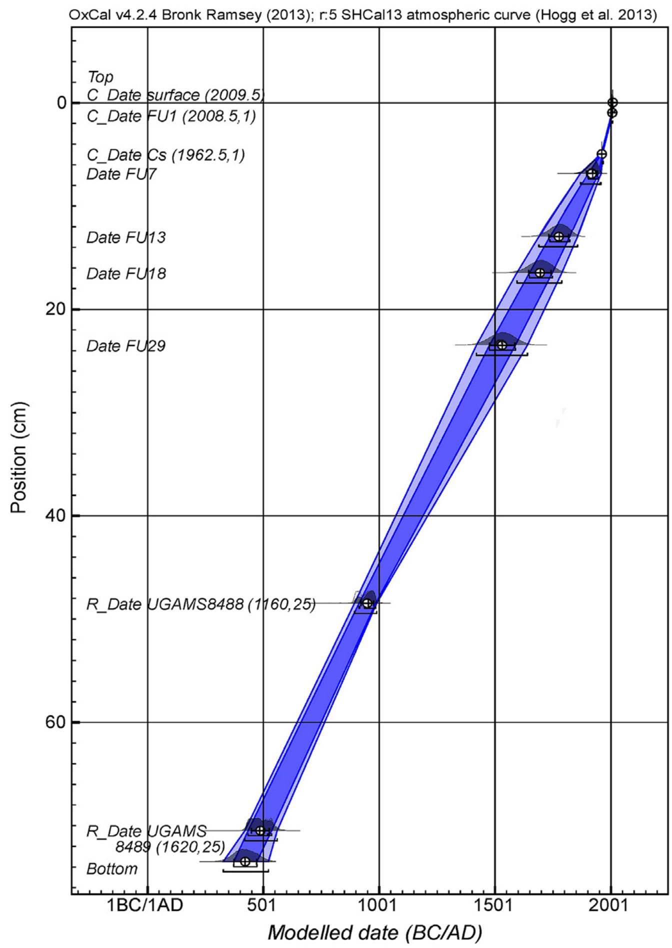

Fig. 4. Age-depth model using OxCal 4.2 (Bronk Ramsey, 2009), with Southern Hemisphere radiocarbon calibration data SHCal13 (Hogg et al., 2013).

darker color and coarser grain size regarding the background sediment (Fig. 4). It was composed mainly of glass shards, scoria fragments, white pumice, and felsic and mafic crystals. Pumice particles (Fig. 5b) with mafic inclusions are relatively scarce and compose the coarser fraction (>500 μm), together with whitish-colorless crystals. These crystals domain the 500-250 μm fraction and correspond mainly to fragments and tabular plagioclase with small opaque inclusions; the dark components of such fraction consist mainly of brown glass shards and black scoria, and minor green to brown prismatic pyroxenes with opaque inclusions. Both felsic and mafic crystaloclast are covered by a vesicular glass coating. Glass shards, and minor scoria fragments, turn into the main components in the <250 μm fraction, giving the dark color to the whole layer.

4.3.3. Tephra FU13

This tephra corresponds to a dark millimetric fine ash layer (12.7–13 cm depth) composed mainly of glass shards, scoria fragments, and white-yellow pumice. Highly vesicular pumice (Fig. 5c) are scarce and forms de coarser fraction (>250 μm), while spongy glass (Fig. 5d) and less vesicular scoria predominate at the <250 μm fractions. Crystals and crystal fragments of plagioclase and pyroxene, and lithics are present in all fractions.

4.3.4. Tephra FU18

This deposit (16.5–18 cm depth) is represented by coarse ash, clearly identified by coarser grain size and lighter color compared with the background sediment. The >500 μm fraction is composed mainly by grayish-white pumiceous particles and felsic crystals, while in the <500 μm fraction dominate felsic crystals and crystal fragments, with minor mafic crystals and lithics, and rare pumice. Whitish pumice have, in average, 2–3 mm length (reaching up to 6 mm) with irregular to sub-rounded shapes, very high vesicularity (Fig. 5e), and common felsic and mafic inclusions. Felsic crystals are composed of white tabular euhedral to subhedral plagioclase with small opaque inclusions; mafic crystals are represented by brownish-greenish elongated pyroxene prisms with opaque inclusions and smaller anhedral amphibole; glomerocrysts are also common. Almost all crystals and glomerocrysts are coated by glass (Fig. 5f). Pumice and crystal particles resemble those previously described components for FU7.

4.3.5. Tephra FU29

This thick deposit (24–29 cm depth) is clearly distinctive in the background sediment due to its dark color and coarser grain size, although corresponding to fine ash. These 5 cm are represented by a composite laminated material with net low contact, formed mainly by glassy particles and scoria. Plagioclase and pyroxene were identified as the main mineral phases. In detail, the layer can be separated in four sub-layers, like repeated deposits of approximately 1 cm thick marked each one by dark bottoms grading to slightly lighter tops, with this light material resembling the background sediment. The observation of the components allowed to discern they correspond to homogeneous material with dominance of volcanic glass shards and scoria fragments rather than heterogeneous layers from reworking. As a whole, the deposit shows normal grading, with maximum grain size reaching few millimeters. The morphology of glass shards showed different features: moderately to highly vesicular irregular shards (Fig. 5g) predominate in the base; shards with lumpy smooth, like molten surfaces, and presence of internal vesicularity prevail in an intermediate position, and such feature is the commonest in the glass shards deposited in the upper centimeter (Fig. 5h–i). This allows inferring successive ash fall deposits instead of reworking and re-deposition of the basal layer. The geochemical analyses of glass shards at different depths (25, 27, and 29 cm depth) showed similar composition (see Section. 4.4); therefore, hereafter the deposit is considered as a unique tephra.

4.4. Geochemical comparison

Different juvenile components were identified in the tephras, namely white pumice, scoria particles, and glass shards. In order to obtain a full characterization, bulk geochemical data was obtained for the different kinds of particles isolated according similar optical features, in the fractions >500 μm and 500-250 μm. Major and trace elements concentrations are listed in Table 3, and selected plots in Figs. 6 and 7 illustrate the compositional differences among tephras, based on variations in magma composition typical for subduction-related volcanoes (Jacques et al., 2014; Wehrmann et al., 2014a, 2014b). The geochemical fingerprint of the tephras showed at least 3 distinctive volcanic sources, grouping all glass shards and scoria (from FU7, FU13, and FU29) in one pattern, and separating two kinds of white pumice (from FU1 and FU13, and from FU7 and FU18; Fig. 6). Tephra ranged in estimated composition from trachybasalts to rhyolites, clustered in three groups corresponding glass and scoria to trachybasalt-basaltic trachyandesite (48–53% SiO_2), one white pumice (from FU7 and FU18) to andesite (62–63% SiO_2), and a second white pumice (from FU1 and FU13) to rhyolite (71–74% SiO_2) (Fig. 6a, Table 3). Taking MgO as evolution index the grouping is defined by 0.32–0.62% MgO, 2.10–2.40%

Table 2
Summary of key physical features of Lake Futalaufquen tephras.

Layer	Position (cm depth)	Sedimentary features, components, and mineralogy
FU1	0-1	Dispersed white pumice in the oxidized upper cm of the core, fine ash reaching 0.5 mm. Domain of highly vesicular white pumice fragments.
FU7	6.5-7	Dark fine ash crystal-rich material with pumice reaching 0.5 mm length, graded contacts (possibly obscured during the sampling). Abundant brown glass shards and scoria fragments; scarce coarser grayish-white pumice with mafic inclusions; glass coated felsic and mafic crystals with opaque inclusions, and glomerocrysts; rare lithics. Pl, px, opaque inclusions.
FU13	12.7-13	Dark millimetric fine ash layer with pumice fragments reaching 0.5 mm length, net low contact. Brown glass shards and scoria fragments, minor coarse white-yellow pumices, domain of felsic crystals and crystals fragments over mafic ones; lithics. Pl, px.
FU18	16.5-18	Grayish-white crystal-rich layer, net low contact, coarse ash with pumice fragments reaching 5-6 mm. Abundant whitish irregular to sub-rounded highly vesicular pumice with felsic and mafic inclusions; glass coated felsic and minor mafic crystaloclast, and glomerocrysts; crystal fragments; lithics. Abundant pl, minor px and amp; opaque inclusions.
FU29	24-29	Dark laminated material, net low contact, normal grading, fine ash. Brown vesicular glass and scoria fragments; glass increase water-magma interaction features to the top; lithics and crystaloclasts. Pl, px.

MgO, and 3.33–3.85% MgO groups (Table 3).

Trace element concentrations (Table 3) showed the same variation patterns, as demonstrate some selected ratios and the chondrite normalized REE (Rare Earth Elements) patterns (McDonough and Sun, 1995) (Fig. 6). Considering the ratio of a highly fluid-mobile to an incompatible immobile element like Ba/Th, glass shards and scoria showed intermediate ratios between the two pumices with lower differentiation when a less fluid-mobile element is considered (Ta/Th) (Fig. 6b). On the other hand, plotting ratios of more to less incompatible immobile elements like La/Yb and fluid-mobile incompatible alkalis as Rb/Cs, glass and scoria showed a higher and more variable alkali content with the lower La/Yb ratio while both kinds of pumice showed less alkalis and higher incompatible element ratios (Fig. 6c). Notably, the lower La/Yb ratio of glasses and scoria corresponds with both light and heavy REE enrichment regarding the two pumices, also the latter with variable La/Yb ratio and REE patterns between them (Fig. 6c–d).

Extended multi-element mantle normalized patterns (McDonough and Sun, 1995) refer to these differences too (Fig. 7a) showing also correlation of tephras with volcanic sources (Fig. 7b–f). The three identified patterns showed, even considering the differences among them, a distinctive subduction-related magma signature characterized by more fluid mobile LILE (Large Ion Lithopile Elements, Cs, Rb, Ba, K) regarding less fluid mobile HFSE (High Field Strength Elements, Ta), light REE enrichment in relation to heavy REE, and different Sr–Ti behavior (Fig. 7a). Comparatively, glass shards and scoria showed intermediate LILE contents but the highest HFS and REE enrichment. For pumices there was an extreme pattern with the highest LILE and lowest HFE and REE contents, while the second pattern showed the lowest LILE and light REE but intermediate middle to heavy REE contents. Consequently, tephras FU1, FU18, and FU29 are clearly differentiated by these parameters due to particle homogeneity, while presence of different kind of particles in FU7 and FU13 resulted in variable compositions related to the other tephras depending on the component considered.

5. Discussion

5.1. Modeled ages and tephra source correlation

5.1.1. Tephra FU1 (AD 2008)

Even though Lake Futalaufquen area was directly affected by 2008 Chaitén volcano eruption, as it was clearly demonstrated by the effects on Esquel town and by the ash dispersion maps (Alfano et al., 2011), this tephra seems to be under-represented in Lake Futalaufquen. This can suggest important within lake processes causing redistribution of the pyroclastic material by lake currents, possibly transporting by overflows or interflows different grain size particles, generating intralake differences in the deposit as were observed, probably in a magnified way, in lakes closer to volcanoes (Van Daele et al., 2014; Bertrand et al., 2014). A similar situation was observed in Lake Rivadavia, approximately 15 km to the North of Lake Futalaufquen, where the deposit was not identified in a short sedimentary sequence (unpublished data). In addition to the stratigraphic position, the chemistry of the pumices is clearly correlated with the characteristic Chaitén rhyolitic products (Figs. 6a and 7b), representing a potential distinctive marker in a wide region considering the ashes geographical distribution (Alfano et al., 2011, Daga et al., 2014).

5.1.2. Tephra FU7 (AD 1890–1940)

The different composition between white pumice and glass and scoria fragments allowed inferring mixing of products from different volcanoes (Fig. 6). Even related in time to the 1890–1920 eruptive cycle from Huequi volcano, the elemental composition of the corresponding products (T2 tephra in Watt et al., 2011b) and FU7 showed clear differences (Figs. 6a and 7c). Noticeable, white pumice from FU7 is similar to FU18 pumices (Figs. 6–7a), correlating geochemically with an older dacitic tephra from Huequi volcano (Figs. 6a and 7c) (T1 in Watt et al., 2011b; see FU18 discussion).

On the other hand, glass shards showed different composition with grain size. The finer glass shards and scoria fragments have the

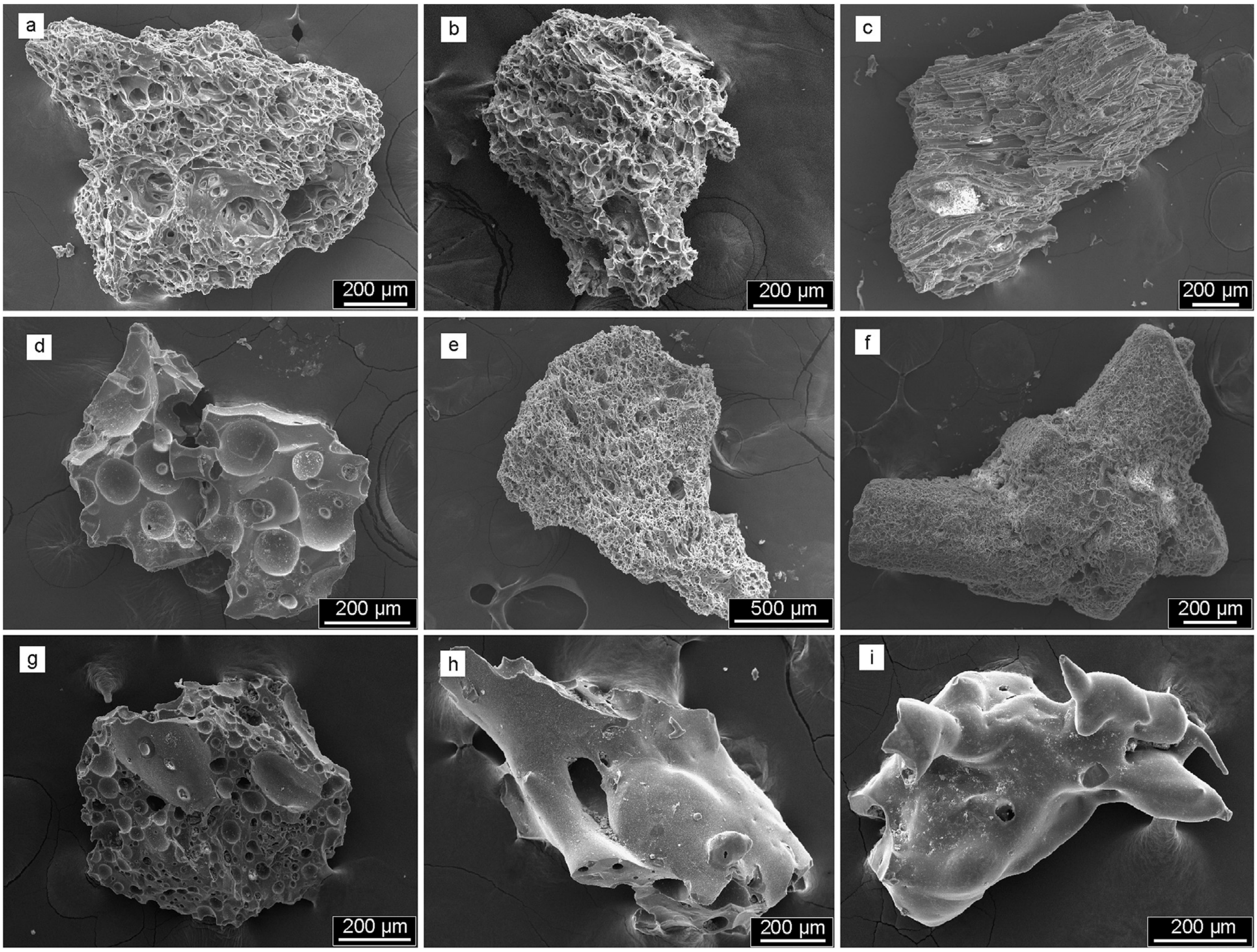

Fig. 5. Scanning Electron Microscopy (SEM) images of volcanic ashes from Lake Futalaufquen tephras: (a, b) highly vesicular white pumice from FU1 and FU7, respectively; (c, d) highly vesicular fluidal white pumice and glass shards with moderate vesicularity, respectively, from FU13; (e, f) highly vesicular white pumice and glass coated glomerocryst, respectively, from FU18; (g) vesicular glass shard irregularly shaped from FU29; (h, i) irregular glass shards with smooth like-molten surfaces from upper part of FU29.

same geochemical signature as those from FU13 and FU29, related to Michinmahuida accessory cones (see FU13 and FU29 discussion; Fig. 7). Although no recent events have been reported in field observations, some older eruptions are mentioned in historical chronicles (Fig. 8). The coarser fraction (FU7b2 in Table 3) showed lower contents in almost all rare earth and incompatible elements (Figs. 6c–7c) showing also similarity with a basalt from Michinmahuida volcano (López Escobar et al., 1993) (Fig. 7c).

The different components were associated with defined sources (Huequi and Michinmauida volcanoes), but the gaps in the historical record in this region do not allow their correlation with known eruptions. The scarce available information from the 1890–1920 Huequi cycle (chronicles mention separate eruptions in 1890–91, 1893–94, 1895–96, 1906, 1917, 1920, and 1922; Petit Breuilh Sepúlveda, 2004, Fig. 8) and the similar products dispersed hundreds years before (see FU18 discussion) do not allow, however, discard such cycle as a possible source for FU7 pumice. Otherwise, although there are no eruptive records during 20th century beginnings from Michinmahuida and accessory cones (Fig. 8), glass shards and scoria could be representing a small and short lived unknown eruption from these sources, not recorded or not identified in the field for that times (Table 4). Glass shards and pumice fragments features did not show strong evidences of transport or long reworking, supporting the hypothesis of FU7 as a record of unknown, or not fully characterized events rather than a reworked layer. Nevertheless, more information about eruptive history of southern SVZ and tephra records from east Andean lakes would help to figure out this kind of multi-sourced tephra layers.

5.1.3. Tephra FU13 (AD 1735–1815)

Geochemical differences between rhyolitic pumice and basaltic glass shards, and their similarity with components in the other tephras, suggested their provenance from different volcanic sources (Fig. 6). Rhyolitic products are not abundant in southern SVZ. Old rhyolites were described from Yate volcano (130 km NNW from Lake Futalaufquen; Watt et al., 2011a, Fig. 8), but the slightly lower silica, higher heavy REE content and differences in fluid-mobile incompatible elements, differentiate Yate's products from FU13 white pumice (Fig. 7d).

Actually, white pumice fraction resembles the major and trace elemental composition of Chaitén volcano, similar to FU1 (Figs. 6a–7d, Table 3). The rhyolitic composition of Chaitén is almost unique in SVZ, considered highly anomalous in a regional context (López-Escobar et al., 1993). Some historical compilations refer to Chaitén events during 1742, 1766, 1834–1835, and 1870 (Petit Breuilh Sepúlveda, 2004, Fig. 8), but no geological evidence

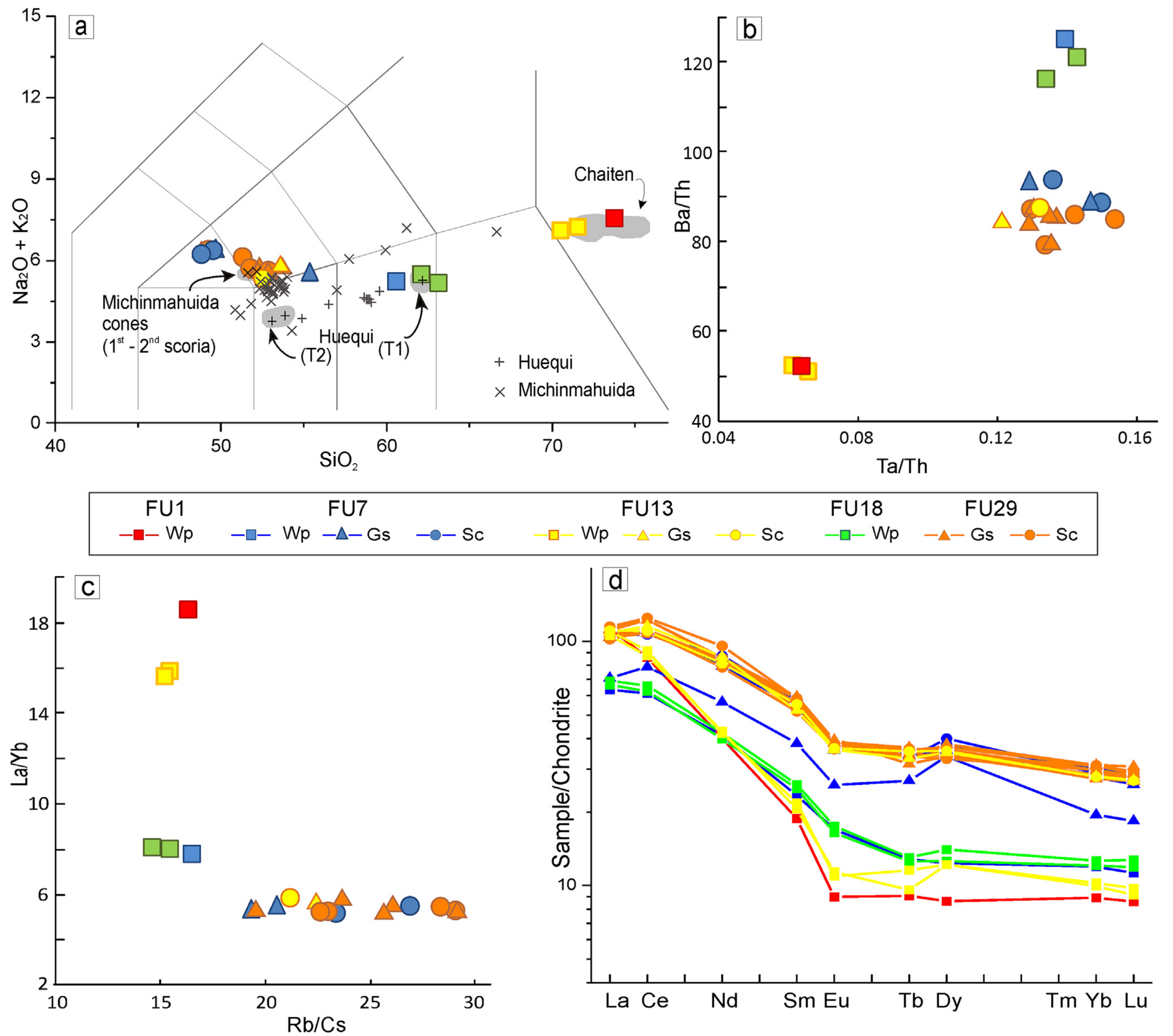

Fig. 6. Selected geochemical diagrams representing bulk compositional variations between tephra layers. (a) TAS plot showing tephras classification compared with the sources identified: Chaitén reference values are shown as a grey area; Huequi and Michinmahuida series are represented by symbols, and samples used for correlation are also grey shaded and clarified in the graph; (b, c) bivariate Ta/Th vs Ba/Th and Rb/Cs vs La/Yb respectively, showed the differences between tephras and between different components (pumice, glass shards, and scoria); (d) REE patterns of different components identified in the tephras, i.e. white pumice (Wp), glass (Gs), and scoria (Sc), normalized to Chondrite (McDonough and Sun, 1995). References: Chaitén: López-Escobar et al. (1993), Stern et al. (2008), Watt et al. (2011a), Ruggieri et al. (2012), Amigo et al. (2013); Huequi: Watt et al. (2011b); Michinmahuida: Amigo et al. (2013).

supports these reports; in fact, historical eruptions from Chaitén volcano, previous to 2008, are just being studied in the last years. A new deposit dated older than AD 1650 (Amigo et al., 2013) was correlated and constrained to AD 1625–1658 by Lara et al. (2013), matching with a historical eruption depicted in old maps for this area during 17th century (Lara et al., 2013). Watt et al. (2013), on the other hand, recognized two small-volume rhyolitic tephra fall deposits (named Cha3 and Cha4) beneath the Chaitén 2008 deposit, separated by a centimeter of organic-rich soils, but they were not dated. Lately, a rhyolitic tephra assigned to AD 1465–1607 was identified in a lake close to the volcano (LTT-2 in Moreno et al., 2014). Except for the correlation between Lara et al. (2013) and Amigo et al. (2013) deposits, the others have not a clear age link, thus being difficult to match them (Fig. 8). According to the age-depth Futalaufquen model, FU13 could be assigned to the end of 18th century. However, the almost identical composition of Chaitén deposits, the scarce information on spatial distribution, and the inherent errors in the dating methods, do not allow establishing if FU13 could match with some of the mentioned deposits or if it corresponds to a more recent unknown eruption, preventing up to now a clear eruptive reconstruction (Table 4).

Glassy and scoria fractions from FU13 showed similar composition as those from FU7 and FU29 (Table 3, Figs. 6 and 7a), comparable to scoria cones in the flanks of Michinmahuida volcano (Fig. 7d). According to different stratigraphic sequences studied around Chaitén and Michinmahuida volcanoes, Amigo et al. (2013) found an undated scoria deposit over the 17th century rhyolitic ash layer, suggesting eruptive activity related to an unknown scoria

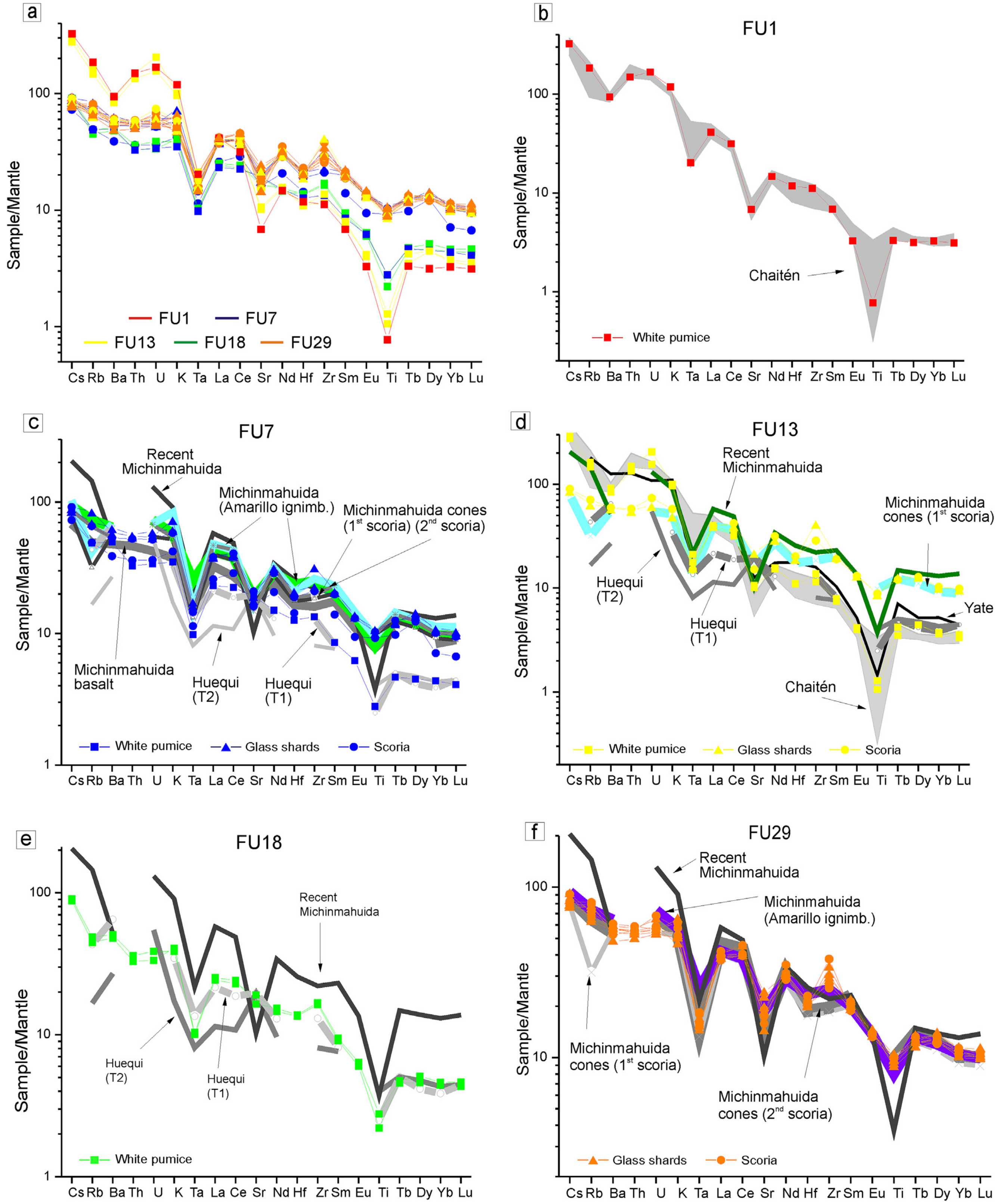

Fig. 7. (a) Multielement diagram representing bulk compositional variations between tephra layers (for symbols refer to each separate tephra); (b, c, d, e, f) Multielement diagrams for FU1, FU7, FU13, FU18, and FU29 (FU29, FU27, and FU25 from Table 3 correspond to FU29 material), respectively, compared with reference data from volcanic sources; reference data compared in the text is plotted for each layer, all normalized to primitive mantle (McDonough and Sun, 1995). References: Chaitén: López-Escobar et al. (1993), Stern et al. (2008), Watt et al. (2011a), Ruggieri et al. (2012), Amigo et al. (2013); Huequi (T1) and Huequi (T2): Watt et al. (2011b); Yate: Watt et al. (2011a); Recent Michinmahuida, 1st and 2nd scoria, and Michinmanuida (Amarillo Ignimbrite): Amigo et al. (2013); Michinmahuida basalt: López Escobar et al., 1993.

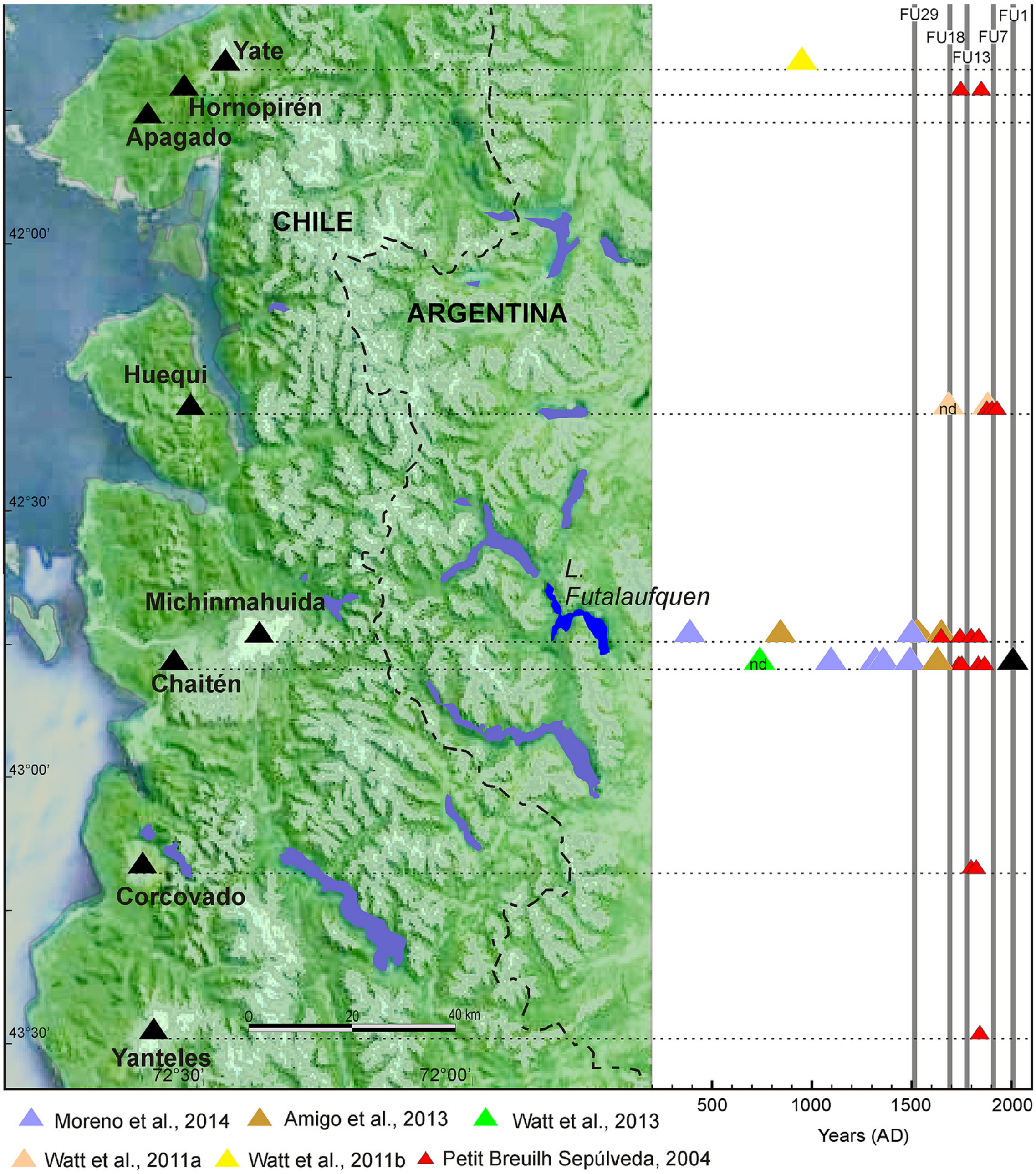

Fig. 8. Volcanoes from the Southern Volcanic Zone between 42° and 43°30′ S, close to the Lake Futalaufquen area, considered in the discussion. On the right side a line-time with eruptions during the last 1800 years is showed. Eruptive record was reconstructed from available information, both from geological evidences as well as historical chronicles. Such historical records are represented by smaller red triangles (Petit Breuilh Sepúlveda, 2004) and they need to be considered carefully. Vertical grey lines correspond to the tephra layers position. (For interpretation of the references to color in this figure legend, the reader is referred to the web version of this article.)

cone eruption (Amigo et al., 2013, Fig. 8). This supports the possibility of unknown eruptions from scoria cones along the LOFZ not only for FU13 but for FU7 too, considering the variable records found in the recent literature and historical chronicles (Fig. 8, Table 4). Therefore, the intensity of the volcanic activity related to scoria cones seems to be underestimated due to the frequent records east from the Andes, or the source should perhaps be reevaluated. More information about SVZ volcanoes and further research in other eastern lakes are necessary to consolidate the results presented here.

5.1.4. Tephra FU18 (AD 1645–1745)

Due to the relative location, the youngest large eruption at Michinmahuida volcano (Fig. 1) was compared with FU18 (Fig. 8). Such subplinian eruption was dated between AD 1450–1650 (Amigo et al., 2013), and corresponds to evolved grey dacitic pumice, but the clear geochemical differences dismissed it as source (Fig. 7e). The comparison with the available information from recent works allowed the correlation of FU18 with a scarcely known tephra from Huequi volcano, located approximately 80 km to the NW of Lake Futalaufquen (Fig. 8) (Watt et al., 2011b). Due to its remote location and difficult access, Huequi volcano has not been studied in detail until Watt et al. (2011b), being particularly

Table 3
Whole rock major and trace element composition of lake Futalaufquen tephras. Oxides as wt % (SiO_2 estimated by difference), trace elements as μg g^{-1}.

Sample	FU1a	FU7a	FU7b2	FU7b3	FU7c2	FU7c3
	White pumice	White pumice	Glass shards		Scoria	
SiO_2	~74	~60	~55	~49	~49	~50
Al_2O_3	13.94	18.59	17.29	18.46	17.44	17.76
TiO_2	0.16	0.56	1.86	2.07	2.18	2.05
Fe_2O_3	1.54	5.59	8.82	10.88	11.58	11.61
MgO	0.32	1.86	3.74	3.51	3.42	3.93
CaO	1.41	6.50	6.22	8.80	8.45	7.43
Na_2O	4.21	4.27	4.28	4.55	4.86	4.59
K_2O	3.43	1.01	1.21	1.69	2.13	1.79
MnO	0.06	0.13	0.20	0.22	0.22	0.22
Sc	2.361 ± 0.092	7.87 ± 0.38	25.9 ± 1.3	33.9 ± 1.2	35.6 ± 1.3	35.5 ± 1.3
V	<5	58.9 ± 8.5	311 ± 17	313 ± 18	318 ± 19	334 ± 18
Cr	4.047 ± 0.56	4.15 ± 0.72	8.3 ± 2.3	5.6 ± 1.8	7.1 ± 2.0	5.2 ± 1.8
Co	1.325 ± 0.084	10.11 ± 0.52	21.2 ± 1.2	26.1 ± 1.4	25.8 ± 1.3	25.8 ± 1.3
Zn	41.6 ± 3.6	74.4 ± 6.7	121.5 ± 14.1	137.5 ± 15.1	133.7 ± 13.2	135.6 ± 12.1
Rb	111.1 ± 8.0	29.3 ± 3.4	29.5 ± 5.5	39.5 ± 6.3	51.2 ± 7.9	42.3 ± 5.8
Sr	136 ± 17	383 ± 42	320 ± 92	417 ± 92	361 ± 69	386 ± 69
Cs	6.84 ± 0.48	1.79 ± 0.18	1.53 ± 0.32	1.93 ± 0.30	1.91 ± 0.30	1.81 ± 0.26
Ba	620 ± 58	327 ± 33	256 ± 52	352 ± 48	387 ± 49	422 ± 52
Zr	117 ± 23	141 ± 43	–	221 ± 91	337 ± 91	241 ± 87
Hf	3.34 ± 0.24	3.59 ± 0.26	4.05 ± 0.35	5.35 ± 0.41	5.99 ± 0.46	5.91 ± 0.45
Ta	0.752 ± 0.063	0.363 ± 0.040	0.421 ± 0.070	0.539 ± 0.064	0.653 ± 0.080	0.611 ± 0.060
Th	11.88 ± 0.66	2.61 ± 0.20	2.87 ± 0.23	4.18 ± 0.33	4.36 ± 0.33	4.49 ± 0.37
Sb	0.600 ± 0.083	0.397 ± 0.080	0.230 ± 0.055	0.212 ± 0.085	0.198 ± 0.085	0.201 ± 0.053
As	11.12 ± 0.78	7.55 ± 0.74	2.85 ± 0.38	3.52 ± 0.79	4.67 ± 0.92	3.87 ± 0.75
Br	1.08 ± 0.17	1.14 ± 0.26	1.06 ± 0.19	1.78 ± 0.38	1.77 ± 0.45	1.60 ± 0.36
U	3.40 ± 0.29	0.687 ± 0.078	0.737 ± 0.096	1.053 ± 0.096	1.10 ± 0.12	1.22 ± 0.11
La	26.75 ± 0.86	15.02 ± 0.65	16.80 ± 0.75	24.73 ± 0.82	25.53 ± 0.87	25.07 ± 0.81
Ce	52.8 ± 3.5	37.6 ± 3.1	48.3 ± 4.2	68.1 ± 5.7	68.0 ± 5.6	65.6 ± 5.3
Nd	18.3 ± 1.7	18.8 ± 1.9	25.8 ± 3.1	36.1 ± 3.7	37.9 ± 3.9	39.9 ± 4.1
Sm	2.78 ± 0.19	3.46 ± 0.29	5.66 ± 0.50	8.06 ± 0.52	8.59 ± 0.54	8.47 ± 0.54
Eu	0.505 ± 0.031	0.957 ± 0.061	1.45 ± 0.13	2.02 ± 0.14	2.09 ± 0.14	2.16 ± 0.19
Tb	0.327 ± 0.028	0.462 ± 0.052	0.97 ± 0.12	1.24 ± 0.12	1.20 ± 0.11	1.22 ± 0.11
Dy	2.12 ± 0.27	3.04 ± 0.33	8.32 ± 0.81	8.83 ± 0.86	9.84 ± 0.98	9.29 ± 0.90
Yb	1.44 ± 0.14	1.92 ± 0.18	3.13 ± 0.32	4.47 ± 0.41	4.65 ± 0.41	4.84 ± 0.42
Lu	0.211 ± 0.018	0.277 ± 0.025	0.452 ± 0.041	0.639 ± 0.052	0.672 ± 0.048	0.708 ± 0.062
Sample	FU13a	FU13a2	FU13b2	FU13c2	FU18a	FU18a2
	White pumice		Glass shards	Scoria	White pumice	
SiO_2	~72	~71	~54	~53	~63	~62
Al_2O_3	15.55	15.87	16.46	16.08	16.33	16.91
TiO_2	0.26	0.21	1.78	1.78	0.44	0.56
Fe_2O_3	1.88	2.10	10.81	12.20	6.02	5.86
MgO	0.43	0.62	3.62	3.80	2.40	2.13
CaO	1.81	2.23	6.68	7.01	5.12	5.60
Na_2O	4.27	4.31	4.15	3.91	4.08	4.45
K_2O	2.89	2.78	1.67	1.43	1.18	1.12
MnO	0.09	0.09	0.21	0.26	0.15	0.14
Sc	3.65 ± 0.13	4.06 ± 0.16	34.5 ± 1.1	33.9 ± 1.2	8.74 ± 0.30	8.70 ± 0.30
V	12.9 ± 4.1	14.4 ± 4.2	278 ± 15	298 ± 14	55 ± 10	61.4 ± 7.6
Cr	5.84 ± 0.76	4.50 ± 0.72	12.0 ± 1.7	9.6 ± 2.1	2.26 ± 0.47	1.84 ± 0.51
Co	2.48 ± 0.14	3.27 ± 0.19	24.3 ± 1.2	30.1 ± 1.5	11.20 ± 0.54	10.86 ± 0.52
Zn	49.0 ± 4.6	44.8 ± 4.8	126.2 ± 12.1	135.6 ± 13.2	85.0 ± 6.8	85.1 ± 6.8
Rb	98.3 ± 7.4	88.0 ± 7.0	42.5 ± 7.1	38.9 ± 5.7	26.9 ± 2.3	29.3 ± 2.6
Sr	201 ± 33	212 ± 34	303 ± 55	438 ± 92	378 ± 41	328 ± 30
Cs	6.38 ± 0.45	5.81 ± 0.42	1.90 ± 0.29	1.84 ± 0.26	1.85 ± 0.14	1.91 ± 0.15
Ba	602 ± 56	554 ± 53	393 ± 51	392 ± 62	318 ± 32	335 ± 34
Zr	120 ± 32	144 ± 44	301 ± 91	441 ± 91	171 ± 27	177 ± 28
Hf	3.14 ± 0.22	3.10 ± 0.23	5.73 ± 0.43	5.47 ± 0.43	3.83 ± 0.27	3.89 ± 0.28
Ta	0.781 ± 0.054	0.657 ± 0.051	0.560 ± 0.074	0.589 ± 0.065	0.374 ± 0.028	0.384 ± 0.029
Th	11.88 ± 0.66	10.66 ± 0.60	4.62 ± 0.29	4.47 ± 0.29	2.62 ± 0.19	2.87 ± 0.17
Sb	0.550 ± 0.082	0.473 ± 0.082	0.182 ± 0.087	0.174 ± 0.078	0.353 ± 0.053	0.361 ± 0.056
As	13.87 ± 1.13	10.79 ± 0.82	4.01 ± 0.59	6.02 ± 1.22	6.72 ± 0.60	7.45 ± 0.74
Br	3.25 ± 0.43	1.72 ± 0.22	1.36 ± 0.46	–	0.97 ± 0.18	1.35 ± 0.27
U	4.15 ± 0.34	3.16 ± 0.29	1.49 ± 0.15	1.27 ± 0.14	0.680 ± 0.062	0.785 0.096
La	26.16 ± 0.89	25.05 ± 0.83	25.81 ± 0.85	26.25 ± 0.89	15.73 ± 0.51	16.33 ± 0.55
Ce	56.1 ± 3.5	53.5 ± 3.4	70.7 ± 4.4	67.6 ± 4.4	38.4 ± 3.2	40.4 ± 2.4
Nd	19.2 ± 1.9	19.6 ± 1.9	39.5 ± 4.4	37.1 ± 3.8	18.2 ± 1.8	19.3 ± 1.9
Sm	3.24 ± 0.25	3.04 ± 0.23	7.73 ± 0.44	8.19 ± 0.52	3.69 ± 0.23	3.84 ± 0.24
Eu	0.614 ± 0.043	0.640 ± 0.048	2.03 ± 0.13	2.05 ± 0.14	0.925 ± 0.053	0.986 ± 0.057

(*continued on next page*)

Table 3 (*continued*)

Sample	FU13a	FU13a2	FU13b2	FU13c2	FU18a	FU18a2
	White pumice		Glass shards	Scoria	White pumice	
Tb	0.417 ± 0.040	0.346 ± 0.037	1.20 ± 0.11	1.28 ± 0.12	0.454 ± 0.034	0.471 ± 0.034
Dy	2.99 ± 0.43	2.99 ± 0.38	8.63 ± 0.85	8.77 ± 0.98	3.10 ± 0.44	3.45 ± 0.44
Yb	1.65 ± 0.16	1.60 ± 0.16	4.52 ± 0.41	4.48 ± 0.43	1.94 ± 0.17	2.04 ± 0.18
Lu	0.240 ± 0.032	0.225 ± 0.022	0.666 ± 0.047	0.661 ± 0.045	0.292 ± 0.021	0.313 ± 0.025

Sample	FU25b2	FU27b	FU27b2	FU27c	FU27c2	FU29b	FU29b2	FU29c	FU29c2
	Glass shards	Glass shards		Scoria		Glass shards		Scoria	
SiO_2	~52	~49	~54	~49	~53	~52	~52	~52	~51
Al_2O_3	16.34	18.06	16.85	17.59	15.93	16.65	16.21	15.82	17.18
TiO_2	1.77	2.09	1.83	2.03	1.98	1.94	1.91	2.00	2.01
Fe_2O_3	11.72	11.72	11.12	11.45	11.15	11.70	11.14	11.62	10.69
MgO	3.31	3.59	3.42	3.33	3.56	3.47	3.43	3.62	3.86
CaO	7.79	7.88	6.05	8.85	7.68	6.89	8.23	8.26	7.59
Na_2O	4.14	4.49	4.33	4.57	4.14	4.29	4.30	4.22	4.47
K_2O	1.46	1.87	1.45	1.78	1.49	1.19	1.34	1.51	1.66
MnO	0.20	0.22	0.21	0.21	0.20	0.22	0.21	0.21	0.22
Sc	33.9 ± 1.2	37.3 ± 1.2	34.3 ± 1.2	35.5 ± 1.3	34.6 ± 1.1	36.2 ± 1.3	35.4 ± 1.3	36.3 ± 1.2	35.1 ± 1.3
V	301 ± 17	315 ± 15	303 ± 15	297 ± 15	305 ± 14	291 ± 15	279 ± 13	296 ± 14	301 ± 15
Cr	1.89 ± 0.91	<3	<3	4.1 ± 2.2	6.20 ± 0.91	9.2 ± 1.6	8.6 ± 1.5	8.2 ± 1.3	7.3 ± 1.8
Co	25.58 ± 0.87	25.6 ± 1.3	24.6 ± 1.2	24.1 ± 1.2	24.6 ± 1.2	25.5 ± 1.2	24.6 ± 1.2	25.8 ± 1.3	24.6 ± 1.2
Zn	140.3 ± 10.4	140.3 ± 15.1	126.2 ± 11.3	133.7 ± 15.1	128.1 ± 11.3	132.8 ± 11.2	124.3 ± 11.3	134.7 ± 12.2	139.4 ± 13.2
Rb	38.8 ± 6.1	46.2 ± 4.4	42.6 ± 5.0	48.8 ± 7.0	47.5 ± 5.8	44.5 ± 5.0	37.4 ± 5.9	43.0 ± 6.3	39.7 ± 4.81
Sr	284 ± 44	365 ± 92	389 ± 87	315 ± 85	351 ± 50	477 ± 92	448 ± 63	380 ± 72	347 ± 61
Cs	1.64 ± 0.21	1.59 ± 0.34	1.64 ± 0.21	1.82 ± 0.28	1.64 ± 0.16	1.74 ± 0.18	1.91 ± 0.24	1.91 ± 0.22	1.73 ± 0.24
Ba	316 ± 39	377 ± 78	360 ± 47	402 ± 81	348 ± 41	391 ± 46	371 ± 55	378 ± 54	377 ± 43
Zr	295 ± 87	–	353 ± 91	–	398 ± 71	306 ± 52	321 ± 73	268 ± 77	282 ± 91
Hf	5.65 ± 0.30	6.11 ± 0.50	5.57 ± 0.42	6.50 ± 0.51	5.94 ± 0.43	6.09 ± 0.44	5.91 ± 0.44	5.73 ± 0.42	6.04 ± 0.45
Ta	0.533 ± 0.041	0.561 ± 0.084	0.564 ± 0.072	0.666 ± 0.081	0.588 ± 0.058	0.622 ± 0.048	0.564 ± 0.049	0.563 ± 0.075	0.680 ± 0.092
Th	3.94 ± 0.24	4.30 ± 0.42	4.18 ± 0.30	4.67 ± 0.31	4.39 ± 0.29	4.54 ± 0.30	4.38 ± 0.30	4.33 ± 0.32	4.43 ± 0.26
Sb	0.177 ± 0.049	0.228 ± 0.077	0.183 ± 0.074	0.201 ± 0.059	0.221 ± 0.062	0.181 ± 0.050	0.244 ± 0.089	0.159 ± 0.070	0.202 ± 0.066
As	2.39 ± 0.59	3.43 ± 0.46	4.57 ± 0.55	3.78 ± 0.49	3.30 ± 0.56	3.61 ± 0.51	2.93 ± 0.46	3.74 ± 0.49	4.07 ± 0.60
Br	1.36 ± 0.48	1.49 ± 0.30	1.52 ± 0.27	1.71 ± 0.38	1.71 ± 0.38	1.44 ± 0.38	1.60 ± 0.30	1.70 ± 0.25	2.01 ± 0.30
U	1.07 ± 0.13	1.14 ± 0.14	1.10 ± 0.13	1.15 ± 0.14	1.20 ± 0.13	1.31 ± 0.16	1.20 ± 0.15	1.15 ± 0.14	1.38 ± 0.14
La	26.68 ± 0.86	26.68 ± 0.86	24.65 ± 0.83	27.22 ± 0.89	24.23 ± 0.78	26.31 ± 0.86	25.75 ± 0.85	25.12 ± 0.77	25.22 ± 0.83
Ce	75.0 ± 4.8	75.0 ± 4.8	66.1 ± 4.1	76.4 ± 4.8	67.5 ± 4.2	75.3 ± 5.0	68.3 ± 4.2	67.8 ± 4.2	66.3 ± 4.0
Nd	39.2 ± 4.4	39.2 ± 4.4	37.5 ± 3.5	43.8 ± 5.0	35.8 ± 3.4	38.9 ± 3.5	38.5 ± 4.0	37.8 ± 3.7	39.2 ± 4.1
Sm	7.72 ± 0.49	8.78 ± 0.52	8.04 ± 0.53	8.65 ± 0.56	7.65 ± 0.42	8.61 ± 0.56	8.12 ± 0.53	8.04 ± 0.54	8.26 ± 0.54
Eu	2.22 ± 0.10	2.22 ± 0.17	2.16 ± 0.13	2.13 ± 0.16	2.04 ± 0.12	2.17 ± 0.12	2.04 ± 0.12	2.10 ± 0.13	2.16 ± 0.14
Tb	1.136 ± 0.085	1.22 ± 0.15	1.22 ± 0.10	1.30 ± 0.15	1.207 ± 0.086	1.327 ± 0.092	1.201 ± 0.092	1.221 ± 0.092	1.311 ± 0.092
Dy	8.33 ± 0.86	9.32 ± 0.93	8.56 ± 0.78	9.06 ± 0.96	8.49 ± 0.85	8.46 ± 0.80	8.66 ± 0.85	8.12 ± 0.75	8.84 ± 0.86
Yb	4.47 ± 0.41	5.01 ± 0.40	4.41 ± 0.40	5.00 ± 0.46	4.58 ± 0.42	4.98 ± 0.45	4.77 ± 0.47	4.80 ± 0.49	4.79 ± 0.43
Lu	0.682 ± 0.053	0.756 ± 0.069	0.659 ± 0.046	0.721 ± 0.056	0.683 ± 0.058	0.707 ± 0.060	0.666 ± 0.053	0.682 ± 0.051	0.693 ± 0.050

interesting for tephrochronological studies because it is considered unusual regionally, with a unique geochemistry within the SVZ (Watt et al., 2011b). The authors describe only two poorly exposed tephra deposits around the volcano: T2, related to the most recent activity between AD 1890–1920, and T1, older than T2 but without age definition (Watt et al., 2011b). Both tephras form a coherent suite with lava samples, but the older identified (T1) shows the most evolved composition of Huequi products (Fig. 6a). FU18 pumices showed high geochemical and mineralogical similarity with the undated T1 tephra (Figs. 6a and 7c), which is described in proximal sites as 1 m bed of white pumice containing fragments of up to 10 cm, suggesting a moderate to large explosive eruption, rich in plagioclase and pyroxene as main phenocryst phases, and amphibole (Watt et al., 2011b), as well as FU18. This layer would represent the first distal record of T1, contributing to the poorly known eruptive history of Huequi volcano and providing evidence of the explosiveness of the event that generated T1. Therefore, it is possible to assign a date of AD 1645–1745 to T1 according to the age depth model of Lake Futalaufquen sequence (Table 4). Further researches in other sites east of the Andes are necessary for a better comprehension of this event distribution pattern.

5.1.5. *Tephra FU29 (AD 1475–1585)*

The youngest pumice from Michinmahuida subplinian eruption is temporally consistent with FU29 dating, around AD 1450–1650 (Amigo et al., 2013), but FU29 components (glass and scoria) and its geochemical composition (Figs. 6 and 7f), are not in agreement with recent dacitic Michinmahuida products. In addition, Amigo et al. (2013) suggested that the Michinmahuida plume may have been transported in a southeast direction, probably not affecting Lake Futalaufquen area. Melimoyu volcano could be considered a potential source due to the geochemical composition (López Escobar et al., 1993), but the location 170 km to the south, and a record of more silicic composition for the youngest known deposit (ca. AD 200, Naranjo and Stern, 2004) led to disregard this option.

Recently, Amigo et al. (2013) identified several scoria deposits associated with scoria cones located on the flanks of Michinmahuida volcano and along the Liquiñe-Ofqui Fault Zone (LOFZ). The two youngest, 1st and 2nd scoria in Amigo et al. (2013), are basaltic trachyandesites (Fig. 6a), correlating with the multielement patterns of FU29 products (Fig. 7f). The 2nd scoria is older than FU29 (AD 650–850; Amigo et al., 2013, Fig. 8) thus it was discarded. Only one geochemical analysis is available for 1st scoria, but the agreement with FU29 tephra is consistent, showing differences in Rb and Zr contents only. In proximal locations, the 1st scoria forms

Table 4
Lake Futalaufquen tephra layers correlation summary.

Layer (cm depth)	Modeled age (cal AD±1σ)	Main features	Source	Correlation
FU1 (0-1)	2008	Dispersed rhyolitic white pumice	Chaitén volcano	Observed event
FU7 (6-7)	1915±25	Trachybasaltic glass shards and scoria;	Scoria cones related to Michinmahuida volcano;	Unknown event?
		Andesitic grayish-white pumice, glass coated plg, px, and glomerocrysts	Huequi volcano	1890-1920 cycle? (Watt et al., 2011b)
FU13 (12.7-13)	1775±40	Basaltic trachyandesitic glass shards and scoria, minor crystals;	Scoria cones related to Michinmahuida volcano;	Unknown event? Scoria over 17th rhyolite? (Amigo et al., 2013)
		Minor rhyolitic white-yellow pumice	Chaitén volcano	17th century (AD 1625-1658)? (Lara et al., 2013) ~AD 1650? (Amigo et al., 2013) Small-volume not dated rhyolitic tephra: Cha3? Cha4? (Watt el al., 2013) LTT2 (AD1465-1607)? (Moreno et al., 2014)
FU18 (16.5-18)	1695±50	Andesitic grayish-white pumice, glass coated plg, px, and glomerocrysts	Huequi volcano	T1 (Watt et al., 2011b)
FU29 (24-29)	1530±55	Basaltic trachyandesitic layered deposit, with dark glass shards and scoria	Scoria cones related to Michinmahuida volcano	1st scoria (Amigo et al., 2013) LTT3? (Moreno et al., 2014)

a 40 cm thick deposit of a pale olive layered scoria varying in thickness and grain size but with similar composition (Amigo et al., 2013). Although the components are not described in the reference, the characteristics of the deposit are comparable with FU29. First scoria deposit resembles a strombolian deposit from several eruptive pulses probably from one of the scoria cones along the LOFZ (Amigo et al., 2013). Considering that present report is situated almost 60 km to the east, perhaps a higher intensity eruption than a strombolian event, or a violent strombolian eruption, should be considered as the source for 1st scoria deposit, representing thus FU29 the first distal record reported of such event. The geochemistry of older products from Michinmahuida volcano, like basaltic andesitic scoria from Amarillo Ignimbrite (Amigo et al., 2013), showed multielement diagrams very similar to FU29 and scoria cone products (Fig. 7f), evidencing the related origin of the magmas. Lately, a coarse-grained basaltic andesitic tephra identified in a lake core close to Chaitén volcano was assigned indistinctly to Michinmahuida volcano and its satellite eruptive center (LTT-3 in Moreno et al., 2014, Fig. 8), possibly related with FU29. The 1st scoria deposit (Amigo et al., 2013) was dated previous to AD 1650, the LTT-3 tephra was assigned at AD 1440–1550 (Moreno et al., 2014), and FU29 tephra was dated in AD 1475–1585 according the age-depth model, showing reasonable agreement between the three records (Table 4). Nevertheless, studies in the previously mentioned scoria cones and the identification of the scoria sources should improve the correlation.

5.2. Extending tephra records

The lack of tephrochronological works in this part of Patagonia and the limited knowledge about the eruptive history of the numerous volcanoes in the southern SVZ introduced some difficulty in the source identification and correlation of the tephra layers from Lake Futalaufquen. Some studies were carried out in recent lake sequences from Nahuel Huapi National Park, 200 km north from Los Alerces National Park, identifying the Cordón Caulle complex, and Osorno and Calbuco volcanoes as the main systems affecting northern Patagonia during the last centuries (Daga et al., 2008, 2010). According to the present results, such volcanoes have not affected Lake Futalaufquen during the time spanned. Works carried out in nearby (40–50 km) northern lakes have focused mainly on paleoenvironmental approaches covering the last 10–14 ky (Iglesias et al., 2011), identifying coarse tephra layers, without enough detail for tephrochronological correlations, particularly during the last centuries. On the other hand, tephrochronological investigations of the southernmost part of SVZ, identified as main events in this area two tephra deposits exposed in road-cuts on the shores of Lake Futalaufquen, which have occurred between 6650 and 5120 yr BP the older one, and between 3840 and 1840 yr BP the youngest (Naranjo and Stern, 2004). These tephras are not temporally related to our results, but they must be considered as possible sources of the available material from the catchment to the water body. According to the authors, both deposits were correlated with Michinmahuida volcano (Naranjo and Stern, 2004), but later, based on the geochemical characterization, Watt et al. (2013) suggested that the youngest was generated by a Holocene Chaitén eruption. Considering this, such thick deposit in open outcrops and under high annual precipitations becomes an important source of Chaitén ashes to the lake, but the similarity between Chaitén products does not allow the discrimination between events. Regarding the older tephra identified by Naranjo and Stern (2004), the reported geochemical composition did not correlate with our results from the proposed mix source tephras either, like FU13 and FU7.

Recent works lead to the study of volcanoes from the Southern SVZ located in remote areas, uninteresting until now or complicated for field expeditions due to difficult access and high forest density at these latitudes. Other studies were prompted mainly by the Chaitén eruption in 2008 to improve the knowledge of volcanic events from a volcano considered almost inactive; furthermore, pyroclastic flows associated to the 2008 Chaitén eruption discovered new outcrops in the area giving the possibility to study previous activity from Chaitén and closer volcanoes. These recent works recognize until now unknown eruptive deposits for the last centuries from Yate, Huequi, Chaitén, and Michinmahuida volcanoes (Watt et al., 2011a, 2011b, 2013; Amigo et al., 2013; Lara et al., 2013; Moreno et al., 2014). Considering all the volcanoes which could affect the area according to geographical location, the geochemical composition became the main parameter for correlation because of the scarce information about eruptive frequency, product dispersion, and eastward deposition. Nevertheless, although the geochemical characterization of the new tephra records is limited and the ages assigned are wide-ranging considering the time spanned, it was possible to generate an outline tephrostratigraphy which may provide a test for future studies.

In this way, tephras identified in Lake Futalaufquen, with a robust chronological framework, can be considered the first records of distal tephra layers recently identified and only just recorded in areas proximal to the sources, mainly from Huequi and Chaitén volcanoes and Michinmahuida accessory cones (Table 4).

6. Conclusions

Detailed characterization of tephra layers is a crucial aspect for tephrochronological applications. The establishment of clear correlations between lacustrine tephra layers and volcanic source in this part of the SVZ resulted in an intricate task, even with a defined chronological framework, due to a general lack of information either from volcanic activity and characterization of known events and their products. Conversely, the definition of a consistent age-depth model allowed the identification and age constraint of the first reported distal tephra records from Huequi and Michinmahuida complex affecting eastern Patagonian territories during last centuries. On the other hand, the apparent absence of clear tephras previous to mid 16th century (up to 5th century) is matter of future debate and study, considering both changes in lake conditions preventing tephra preservation or the decrease in eruptive frequency. Nevertheless, further research is necessary, particularly in lake sequences east of the Andes, to better understand the historical record of closer volcanoes, allowing for more complete dispersion patterns and affected areas. This represents an important fact from the volcanic risk approach, with the example of Chaitén volcano, assumed to be almost inactive until the last 2008 eruption; although considering the unique character of this volcano generating highly explosive eruptions, other closer volcanoes should not be underestimated in hazard evaluations.

Acknowledgments

The authors wish to express their gratitude to Andrea Rizzo and Ricardo Sánchez for their collaboration in sampling and sample conditioning, to the Grupo de Caracterización de Materiales del Centro Atómico Bariloche for the support in the SEM and DRX studies, to the reactor RA-6 operation staff for their assistance in sample analysis, and to Alejandro Demichelis for valuable comments on mineralogy and geochemistry. We are grateful to Leonardo Buria (National Parks Administration) and personal from Los Alerces National Park for fieldwork supporting. We also thank to David Pyle and an anonymous reviewer for their valuable comments at the revision stage, improving the quality of the original manuscript. This work was partially funded by SeCTyP 06/C339, Fundación Balseiro (2010/2011) and PICT 2012-280 projects.

Appendix A. Supplementary data

Supplementary data related to this article can be found at http://dx.doi.org/10.1016/j.jsames.2015.12.003.

References

Alfano, F., Bonadonna, C., Volentik, A.C., Connor, C.B., Watt, S.F., Pyle, D.M., Connor, L.J., 2011. Tephra stratigraphy and eruptive volume of the May, 2008,Chaitén eruption, Chile. Bull. Volcanol. 73, 613–630.

Amigo, A., Lara, L., Smith, V., 2013. Holocene record of large explosive eruptions from Chaitén and Michinmahuida Volcanoes, Chile. Andean Geol. 40, 227–248.

Arnaud, F., Magand, O., Chapron, E., Bertrand, S., Boes, X., Charlet, F., Mélieres, M.A., 2006. Radionuclide dating (^{210}Pb, ^{137}Cs, ^{241}Am) of recent lake sediments in a highly active geodynamic setting (Lakes Puyehue and Icalma-Chilean Lake District). Sci. Total Environ. 366, 837–850.

Bertrand, S., Daga, R., Bedert, R., Fontijn, K., 2014. Deposition of the 2011–2012 Cordón Caulle tephra (Chile, 40°S) in lake sediments: Implications for tephrochronology and volcanology. J. Geophys. Res. 119, 2555–2573.

Bronk Ramsey, C., 2008. Deposition models for chronological records. Quat. Sci. Rev. 27, 42–60.

Bronk Ramsey, C., 2009. Bayesian analysis of radiocarbon dates. Radiocarbon 51, 337–360.

Chambers, F., Daniell, J., Hunt, J., Molloy, K., O'Connell, M., 2004. Tephrostratigraphy of an Loch Mór, Inis Oírr, western Ireland: implications for Holocene tephrochronology in the northeastern Atlantic region. Holocene 14, 703–720.

Daga, R., Ribeiro Guevara, S., Sánchez, M.L., Arribére, M., 2006. Geochemical characterization of volcanic ashes from recent events in Northern Patagonia Andean Range by INAA. J. Radioanal. Nucl. Chem. 270, 677–694.

Daga, R., Ribeiro Guevara, S., Sánchez, M.L., Arribére, M., 2008. Source identification of volcanic ashes by geochemical analysis of well preserved lacustrine tephras in Nahuel Huapi National Park. Appl. Radiat. Isotopes 66, 1325–1336.

Daga, R., Ribeiro Guevara, S., Sánchez, M.L., Arribére, M., 2010. Tephrochronology of recent events in the Andean Range (Northern Patagonia): spatial distribution and provenance of lacustrine ash layers in the Nahuel Huapi National Park. J. Quat. Sci. 25, 1113–1123.

Daga, R., Ribeiro Guevara, S., Poiré, D., Arribére, M.A., 2014. Characterization of tephras dispersed by recent eruptions of volcanoes Calbuco (1961), Chaitén (2008), and Cordón Caulle complex (1960 and 2011), in Northern Patagonia. J. S. Am. Earth Sci. 49, 1–14.

Del Valle, H., 1998. Patagonian soils: a regional synthesis. Ecol. Austral 8, 103–123.

Fey, M., Korr, C., Maidana, N., Carrecedo, M., Corbella, H., Dietrich, S., Haberzettl, T., Kuhn, G., Lücke, A., Mayr, C., Ohlendorf, C., Paez, M., Quintana, F., Schäbitz, F., Zolitschka, B., 2009. Palaeoenvironmental changes during the last 1600 years inferred from the sediment record of a cirque lake in southern Patagonia (Laguna Las Vizcachas, Argentina). Palaeogeogr. Palaeoclimatol. Palaeoecol. 281, 363–375.

Fontaine, C.S., Kaufman, D.S., Anderson, R.S., Werner, A., Waythomas, C.F., Brown, T.A., 2007. Late Quaternary distal tephra-fall deposits in lacustrine sediments, Kenai Peninsula, Alaska. Quat. Res. 68, 64–78.

Fontijn, K., Lachowycz, S.M., Rawson, H., Pyle, D.M., Mather, T.A., Naranjo, J.A., Moreno-Roa, H., 2014. Late Quaternary tephrostratigraphy of southern Chile and Argentina. Quat. Sci. Rev. 89, 70–84.

Furci, H., Arribére, M.A., Ribeiro Guevara, S., 2013. Self-shielding corrections in cylindrical samples in gamma spectrometry with germanium well-type detectors. Nucl. Instrum. Methods Phys. Res. Sect. A 705, 132–139.

González-Ferrán, O., 1995. Volcanes de Chile. Instituto Geográfico Militar de Chile, Santiago de Chile.

Heiri, O., Lotter, A.F., Lemcke, G., 2001. Loss on ignition as a method for estimating organic and carbonate content in sediments: reproducibility and comparability of results. J. Paleolimnol. 25, 101–110.

Hogg, A., Hua, Q., Blackwell, P., Niu, M., Buck, C., Guilderson, T., Heaton, T., Palmer, J., Reimer, P., Reimer, R., Turney, C., Zimmerman, S., 2013. SHCal13 southern hemisphere calibration, 0-50,000 years Cal BP. Radiocarbon 55, 1889–1903.

Iglesias, V., Whitlock, C., Bianchi, M.M., Villarosa, G., Outes, V., 2011. Holocene climate variability and environmental history at the Patagonian forest/steppe

ecotone, Lago Mosquito (42°29'37.89'S, 71°24'14.57'W) and Laguna del Cóndor (42°20'47.22'S, 71°17'07.62'W). Holocene 22, 1297–1307.
Jacques, G., Hoernle, K., Gill, J., Wehrmann, H., Bindeman, I., Lara, L., 2014. Geochemical variations in the Central Southern Volcanic Zone, Chile (38–43°S): the role of fluids in generating arc magmas. Chem. Geol. 371, 27–45.
Joshi, S.R., Shukla, B.S., 1991. Ab initio derivation of formulations for ^{210}Pb dating of sediments. J. Radioanal. Nucl. Chem. 148, 73–79.
Lara, L.E., Moreno, R., Amigo, A., Hoblitt, R.P., Pierson, T.C., 2013. Late Holocene history of Chaitén Volcano, new evidence for a 17th century eruption. Andean Geol. 40, 249–261.
Lizuain, A., 1999. Estratigrafía y evolución geológica del Jurásico y Cretácico de la Cordillera Patagónica Septentrional. In: Geología Argentina, Anales, 29, pp. 433–443.
López-Escobar, L., Kilian, R., Kempton, P., Tagiri, M., 1993. Petrography and geochemistry of Quaternary rocks from the Southern Volcanic Zone between 41°30' and 46°00' S, Chile. Rev. Geol. Chile 20, 35–55.
Lowe, D., 2011. Tephrochronology and its application: a review. Quat. Geochronol. 6, 107–153.
McDonough, W.F., Sun, S., 1995. The composition of the Earth. Chem. Geol. 120, 223–253.
Moernaut, J., Van Daele, M., Heirman, K., Fontijn, K., Strasser, M., Pino, M., Urrutia, R., De Batist, M., 2014. Lacustrine turbidites as a tool for quantitative earthquake reconstruction: new evidence for a variable rupture mode in south central Chile. J. Geophys. Res. Solid Earth 119, 1607–1633. http://dx.doi.org/10.1002/2013JB010738.
Moreno, P.I., Alloway, B.V., Villarosa, G., Outes, V., Henríquez, W.I., De Pol-Holz, R., Pearce, N.J.G., 2014. A past-millennium maximum in postglacial activity from Volcán Chaitén, southern Chile. Geology. http://dx.doi.org/10.1130/G36248.1.
Naranjo, J., Stern, C., 2004. Holocene tephrochronology of the southernmost part (42°30'-45°S) of the Andean Southern Volcanic Zone. Rev. Geol. Chile 31, 225–240.
Okuno, M., Nakamura, T., 2003. Radiocarbon dating of tephra layers: recent progress in Japan. Quat. Int. 105, 49–56.
Parnell, A., Buck, C.E., Doan, T.K., 2011. A review of statistical chronology models for high-resolution, proxy-based Holocene palaeoenvironmental reconstruction. Quat. Sci. Rev. 30, 2948–2960.
Paruelo, J.M., Beltrán, A., Jobbágy, E., Sala, O.E., Golluscio, R.A., 1998. The climate of Patagonia: general patterns and controls on biotic processes. Ecol. Austral 8, 85–101.
Petit-Breuilh Sepúlveda, M.E., 2004. La historia eruptiva de los volcanes hispanoamericanos (siglos XVI al XX). In: Serie Casa de los Volcanes No. 8. Ed.. Servicio de Publicaciones Exmo. Cabildo Insular de Lanzarote, Huelva, Spain.
Pizzolón, L., 1995. Lago futalaufquen. In: Calcagno, A., Fioriti, M., Pedrozo, F., Vigliano, P., López, H., Rey, C., Razquin, M., Quirós, R. (Eds.), Catálogo de lagos y embalses de la Argentina.
Ribeiro Guevara, S., Arribére, M., 2002. ^{137}Cs dating of sedimentary cores from lakes of Nahuel Huapi National Park, Patagonia, Argentina, historical records and profile measurements. J. Radioanal. Nucl. Chem. 252, 37–45.
Ribeiro Guevara, S., Rizzo, A., Sánchez, R., Arribére, M., 2003. ^{210}Pb fluxes in sediment layers sampled from Northern Patagonia lakes. J. Radioanal. Nucl. Chem. 258, 583–595.
Robbins, J.A., Herche, L.R., 1993. Models and uncertainty in ^{210}Pb dating of sediments. Radiochem. Limnol. 25, 217–222.
Roig, F.A., Villalba, R., 2008. Understanding climate from patagonian tree rings. Dev. Quat. Sci. 11, 411–435.
Ruggieri, F., Fernandez Turiel, J., Saavedra, J., Gimeno, D., Polanco, E., Amigo, A., Galindo, G., Caselli, A., 2012. Contribution of volcanic ashes to the regional geochemical balance: the 2008 eruption of Chaitén volcano, Southern Chile. Sci. Total Environ. 425, 75–88.
Shane, P., 2000. Tephrochronology: a New Zealand case study. Earth Science Rev. 49, 223–259.
Smol, J.P., 2008. Pollution of Lakes and Rivers, a Paleoenvironmental Perspective. Blackwell Publishing, USA, p. 383.
Steinhauser, G., Sterba, J.H., Bichler, M., 2007. Chemical fingerprints of pumice from Cappadocia (Turkey) and Kos (Greece) for archaeological applications. Appl. Radiat. Isotopes 65, 488–503.
Stern, C., 2004. Active Andean volcanism: its geologic and tectonic setting. Rev. Geol. Chile 31, 161–206.
Stern, C., Navarro, X., Pino, J., Vega, R., 2008. Nueva fuente de obsidiana en la región de la Araucanía, centro-sur de Chile: química y contexto arqueológico de la obsidiana riolítica negra de los Nevados de Sollipulli. Magallania 36, 185–193.
Van Daele, M., Moernaut, J., Silversmit, G., Schmidt, S., Fontijn, K., Heirman, K., Vandoorne, W., De Clercq, M., Van Acker, J., Wolff, C., Pino, M., Urrutia, R., Roberts, S.J., Vincze, L., De Batist, M., 2014. The 600 yr eruptive history of Villarrica Volcano (Chile) revealed by annually laminated lake sediments. Geol. Soc. Am. Bull. 126, 481–498. http://dx.doi.org/10.1130/B30798.1.
Van Daele, M., Moernaut, J., Doom, L., Boes, E., Fontijn, K., Heirman, K., Vandoorne, W., Hebbeln, D., Pino, M., Urrutia, R., Brümmer, R., De Batist, M., 2015. A comparison of the sedimentary records of the 1960 and 2010 great Chilean earthquakes in 17 lakes: implications for quantitative lacustrine palaeoseismology. Sedimentology 62, 1466–1496.
Vila, A., Borrelli, L., 2011. Cattle in the Patagonian forests: feeding ecology in Los Alerces National Reserve. For. Ecol. Manag. 261, 1306–1314.
Wastegard, S., 2005. Late Quaternary tephrochronology of Sweden: a review. Quat. Int. 130, 49–62.
Watt, S.F., Pyle, D.M., Naranjo, J.A., Rosqvist, G., Mella, M., Mather, T.A., Moreno, H., 2011a. Holocene tephrochronology of the Hualaihue region (Andean southern volcanic zone, ~42°S), southern Chile. Quat. Int. 246, 324–343.
Watt, S.F., Pyle, D., Mather, T., 2011b. Geology, petrology and geochemistry of the dome complex of Huequi volcano, southern Chile. Andean Geol. 38, 335–348.
Watt, S.F., Pyle, D., Mather, T., 2013. Evidence of mid- to late Holocene explosive rhyolitic eruptions from Chaitén Volcano, Chile. Andean Geol. 40, 216–226.
Wehrmann, H., Hoernle, K., Garbe-Schönberg, D., Jacques, G., Mahlke, J., Schumann, K., 2014a. Insights from trace element geochemistry as to the roles of subduction zone geometry and subduction input on the chemistry of arc magmas. Int. J. Earth Sci. 103, 1929–1944.
Wehrmann, H., Hoernle, K., Jacques, G., Garbe-Schönberg, D., Schumann, K., Mahlke, J., Lara, L., 2014b. Volatile (sulphur and chlorine), major, and trace element geochemistry of mafic to intermediate tephras from the Chilean Southern Volcanic Zone (33-43°S). Int. J. Earth Sci. 103, 1945–1962.
Wulf, S., Kraml, M., Brauer, A., Keller, J., Negendank, J., 2004. Tephrochronology of the 100 ka lacustrine sediment record of Lago Grande di Monticchio (southern Italy). Quat. Int. 122, 7–30.